Atmos. Chem. Phys. Discuss., https://doi.org/10.5194/acp-2018-1030
Manuscript under review for journal Atmos. Chem. Phys.
Discussion started: 26 November 2018

Atmospheric Chemistry and Physics Discussions

Seasonal characteristics of chemical and dynamical transports into the extratropical upper troposphere/lower stratosphere

Yoichi Inai[1], Ryo Fujita[1], Toshinobu Machida[2], Hidekazu Matsueda[3], Yousuke Sawa[3], Kazuhiro Tsuboi[3], Keiichi Katsumata[2], Shinji Morimoto[1], Shuji Aoki[1], Takakiyo Nakazawa[1]

[1]Center for Atmospheric and Oceanic Studies, Graduate School of Science, Tohoku University, Sendai, 980-8578, Japan
[2] National Institute for Environmental Studies, Tsukuba, 305-8506, Japan
[3] Meteorological Research Institute, Tsukuba, 305-0052, Japan

Correspondence to: Yoichi Inai (yoichi_inai@tohoku.ac.jp)

Abstract. To investigate the seasonal characteristics of chemical tracer distributions in the extratropical upper troposphere and lower stratosphere (ExUTLS) as well as stratosphere–troposphere exchange processes, mixing fractions of air masses originating in the stratosphere, tropical troposphere, mid-latitude lower troposphere (LT), and high-latitude LT in the ExUTLS are estimated using 90-day backward trajectories calculated with European Centre For Medium-Range Weather Forecasts (ECMWF) ERA-Interim data as the meteorological input. Time-series of chemical tracers obtained from ground-based and airborne observations are incorporated into the estimated mixing fractions, thus reconstructing spatiotemporal distributions of chemical tracers in the ExUTLS. The reconstructed tracer distributions are analysed with the mixing fractions and the stratospheric age of air (AoA) estimated using a 10-year backward trajectory. The reconstructed distributions of CO and CO_2 in the ExUTLS are affected primarily by tropospheric air masses because of the short chemical lifetime of the former and large seasonal variations in the troposphere of the latter. Distributions of CH_4, N_2O, and SF_6 are controlled primarily by seasonally varying air masses transported from the stratosphere. For CH_4 and N_2O distributions, air masses transported via the deep branch of the Brewer–Dobson circulation are particularly important. This interpretation is qualitatively and quantitatively supported by the estimated spatiotemporal distributions of AoA.

1 Introduction

The extra-tropical upper troposphere and lower stratosphere (ExUTLS; e.g., Gettelman et al., 2011) accounts for about 40 % of the total stratospheric air mass (Appenzeller et al., 1996) and about 20 % of stratospheric aerosols (Andersson et al., 2015). Trace gases and aerosols in the ExUTLS play an important role in atmospheric radiative processes, especially in the Arctic climate. These species are transported to the ExUTLS from the deep stratosphere via stratospheric residual circulation (Brewer–Dobson circulation, BDC; Brewer, 1949; Dobson, 1956) and from the lower troposphere or the tropical troposphere via local convection, frontal cyclones, Rossby wave breaking in the subtropical jet, monsoon activity, and other systems (e.g.,

Holton et al., 1995; Wernli and Bourqui, 2002; Manney et al., 2011; Pan et al., 2016; Vogel et al., 2016; Boothe and Homeyer, 2017; Ploeger et al., 2017).

Air-mass transport processes into the ExUTLS are strongly dependent on the season. This leads to stratospheric and tropospheric mixing fractions that show clear seasonality. For example, Appenzeller et al. (1996) estimated the mass flux across the 380 K isentrope due to global-scale meridional circulation and found that the downwelling mass flux from the stratosphere varies from 8×10^9 kg s^{-1} in summer to 15×10^9 kg s^{-1} in winter, whereas the Asian summer monsoon and local convection, which supply tropospheric air to the ExUTLS, are active only during the summer and early autumn (e.g., Randel and Park, 2006; Randel et al., 2010). The composition of air masses transported from the deep stratosphere, lower troposphere, and tropical troposphere also shows seasonal variations (e.g., Boenisch et al., 2009). The seasonal variability in air-mass composition and mass-flux strength makes it difficult to essentially understand the distributions of trace gases in the ExUTLS and to describe their transport into the layer.

This study focuses on mixing fractions of air masses originating in the high-latitude stratosphere, tropical troposphere, mid-latitude lower troposphere (LT), and high-latitude LT in the ExUTLS, based on the trajectory analysis of Inai (2018). Using estimated mixing fractions, the transport of chemical species into the ExUTLS and the spatiotemporal distributions of methane (CH_4), nitrous oxide (N_2O), carbon monoxide (CO), sulphur hexafluoride (SF_6), and carbon dioxide (CO_2) in the layer are reconstructed with the aid of atmospheric trace-gas observations including aircraft measurements, such as those of the Comprehensive Observation Network for TRace gases by AIrLiner (CONTRAIL; Nakazawa et al., 1993; Matsueda and Inoue, 1996; Ishijima et al., 2001; Matsueda et al., 2002; Machida et al., 2008; Umezawa et al., 2014; Sawa et al., 2015). Reconstructed distributions for the five species are discussed in terms of dynamical transport, using the stratospheric age of air (AoA) as an indicator of air mass transport via the deep and shallow branches of the BDC.

2 Methods

2.1 Estimating the mixing fraction and age of air

The CONTRAIL data were obtained by collecting air samples once a month from April 2012 to December 2016 at longitudinal intervals of 10° or 15° along individual flight tracks at around 11 km altitude between France/Russia and Japan. The period and longitudinal locations of this analysis were selected based on the CONTRAIL measurements, for which air sampling in the ExUTLS was usually made over Siberia. To identify the origins of ExUTLS air masses, kinematic backward trajectories are calculated for 90 days following the method of Inai (2018). Trajectories are initialized at uniformly distributed grid points (5.0° longitude × 2.5° latitude) within 45° N–80° N and 0° E–140° E at geopotential heights of 5, 6, 7, 8, 9, 10, 11, 12, 13, 14, 15, and 16 km (Fig. 1). Initializations are made at 00:00 UTC on the 5th, 15th, and 25th of every month from January 2012 to December 2016, and use meteorological conditions prescribed by the European Centre For Medium-Range Weather Forecasts (ECMWF) ERA-Interim dataset (0.75° × 0.75° horizontal resolution, 6 hourly temporal resolution, and 60 model levels; Dee et al., 2011). An example of the results is provided in Fig. 2, which shows where particles located as shown in Fig. 1 at 00Z

Atmos. Chem. Phys. Discuss., https://doi.org/10.5194/acp-2018-1030
Manuscript under review for journal Atmos. Chem. Phys.
Discussion started: 26 November 2018

on 15 January 2015 were located 90 days prior (i.e., 00Z on 20 October 2014). Many particles ending up at altitudes greater than 13 km (orange dots) travelled from the mid- or high-latitude stratosphere, above 18 km. However, many particles ending up at altitudes below 10 km (purple to blue-green dots) originated near 10 km, typically in the troposphere. The distribution of some of the particles (green and yellow dots) in the troposphere near ~10° N (upper right panel of Fig. 2) suggests significant vertical transport from the LT to the UTLS in this latitudinal region.

Trajectories obtained from each run are categorized into several groups (trj_k; k = 1 to $kmax$) with criteria (hereafter denoted cri_k) of potential temperature, latitude, potential vorticity, and geopotential height along each trajectory. In this analysis, $kmax$ is set to 5, with k = 1 for the high-latitude stratosphere, k = 2 for the tropical troposphere, k = 3 for the mid-latitude LT, k = 4 for the high-latitude LT, and k = 5 for all other trajectories. Criteria for each k are summarized in Table 1. Note that mixing fractions in the high-latitude stratosphere (k = 1) that have passed through the deep (k = 1a) and shallow (k = 1b) branches of the BDC are evaluated separately using 10-year trajectory calculations with the coarse meteorological data described below. Air masses in the fifth group (k = 5) are considered to be of the tropical and extratropical UTLS, because for at least 90 days they are classified into neither the LT (all latitudes) nor the stratosphere (high latitudes) groups. Trajectories were categorized as trj_k, according to the first set of 3 continuous days along the trajectory that satisfied the cri_k, except for k = 5. Trajectories trj_k are assumed to travel along their own pass ways from origin k to the initial position of the backward trajectory. Mixing fractions of air parcels with origin k (hereafter denoted f_k) are calculated as a function of equivalent latitude ($\emptyset_{eq}$), potential temperature (θ), and month ($\mathcal{M}$) of their release. Denoting as N_k the number of trajectories, which are classified into trj_k groups with distinct $\emptyset_{eq}$, θ, and $\mathcal{M}$, the mixing fraction for origin k is given by

$$f_k = \frac{\sum_{i=1}^{N_k} \rho_{trj_k ini}(i) * \cos \emptyset_{trj_k ini}(i)}{\sum_{k=1}^{kmax} (\sum_{i=1}^{N_k} \rho_{trj_k ini}(i) * \cos \emptyset_{trj_k ini}(i))}, \quad (1)$$

where $\emptyset_{trj_k ini}$ and $\rho_{trj_k ini}$ indicate the initial latitude and density of the individual backward trajectories, respectively. Note that $\rho_{trj_k ini}$ is calculated from the equation of state.

Similar methods are used to estimate the AoA, which is calculated as the average elapsed time until a trajectory goes back to the troposphere where satisfies whichever criteria k = 2, 3, or 4. In this calculation, the coarser ERA-Interim data (1.5° × 1.5° horizontal resolution, 6 hourly temporal resolution, and 37 pressure levels) are used to reduce the computational burden, as the calculation period extends to 10 years. Results of a sensitivity analysis indicate that estimated mixing fractions are independent of the resolution of the input data (see Appendix A). However, Inai (2018) found that the AoA evaluated from a trajectory analysis using the same ERA-Interim data as used in this work is roughly 70 % of the actual value in the mid-latitude stratosphere. To address this underestimation, AoA calculated here are multiplied by a correction factor of 1.43 (the reciprocal of 0.7). The AoA for air masses originating in the high-latitude stratosphere and UTLS are also evaluated only using $trj_{k=1}$ for the former and $trj_{k=5}$ for the latter. The 10-year trajectories are also used to determine whether trajectories categorized as $trj_{k=1}$ passed through the deep or shallow branch of the BDC (k = 1a or 1b). These trajectories are classified as the shallow

Atmos. Chem. Phys. Discuss., https://doi.org/10.5194/acp-2018-1030
Manuscript under review for journal Atmos. Chem. Phys.
Discussion started: 26 November 2018

branch if they cross 380 K but do not reach 30 hPa within 4 years, and as the deep branch if they exceed 30 hPa within 4 years, following the method of Lin et al. (2015).

2.2 Air-mass original composition and reconstruction

The relative abundance of chemical species in the ExUTLS is strongly affected by changes in the breakdown of transported air masses, reflecting the fact that air-mass chemical composition varies with origin. For example, low-latitude tropospheric air masses have relatively high N_2O mixing ratios, whereas high-latitude stratospheric air masses have low mixing ratios, because N_2O sources and sinks exist in the troposphere and the stratosphere, respectively. According to Inai (2018), the mixing ratio of chemical species S in the ExUTLS (X^S) can be reconstructed as a function of $\emptyset_{eq}$, θ, and $\mathcal{M}$ in combination with f_k and the chemical transport from origin k ($X^S{}_k$):

$$X^S = \sum_{k=1}^{kmax} f_k * X^S{}_k. \quad (2)$$

By expressing the mixing ratio of S for an air mass originating in region k ($\equiv X^S{}_{ORG_k}$) as a function of month $\mathcal{M}$ and the elapsed time of trajectory $trj_k(i)$ since leaving its origin k ($\equiv \tau_k(i)$), X^S is calculated as a function of $\emptyset_{eq}$, θ, and $\mathcal{M}$ as follows:

$$X^S(\mathcal{M}) = \sum_{k=1}^{kmax} \frac{\sum_{i=1}^{N_k} X^S{}_{ORG_k}(\mathcal{M}-\tau_k(i)) * \rho_{trj_k ini(i)} * \cos\emptyset_{trj_k ini(i)}}{\sum_{i=1}^{N_k} \rho_{trj_k ini(i)} * \cos\emptyset_{trj_k ini(i)}}. \quad (3)$$

As the time series $X^S{}_{ORG_k}$ should be treated climatologically for each k and S, as required for the mixing fraction f_k, it is necessary to detrend their values. In this study, detrending is applied to the observed values for k = 2, 3, and 4 in which a linear trend is determined for each dataset for the period 2012–2016 and all the observed values are normalized to those on January 2016. Data observed at around 11 km over 10° N–30° N using aircraft flying between Japan and Australia (Matsueda and Inoue, 1996; Matsueda et al., 2002) are used for k = 2, and monthly aircraft data collected by Tohoku University (TU; Nakazawa et al., 1993; Ishijima et al., 2001; Umezawa et al., 2014) at around 2 km over the Pacific Ocean off the coast of Sendai, Japan are employed for k = 3 after taking a 3-month running average. For k = 4, ground-based monthly mean data measured by NOAA/ESRL (National Oceanic and Atmospheric Administration/Earth System Research Laboratory) at Summit, Greenland (SUM) and Barrow, Alaska (BRW) are used after averaging the data from the two stations. N_2O and SF_6 data at the both sites and CH_4 and CO_2 data at BRW were continuously measured in-situ, while other data were obtained using flask sampling method (Dutton et al., 2017; Thoning et al., 2017; Dlugokencky et al., 2018a, 2018b, 2018c; Petron et al., 2018). These data are distributed by the World Meteorological Organization (WMO) World Data Centre for Greenhouse Gases (WDCGG; https://gaw.kishou.go.jp/).

The time series $X^S{}_{ORG_k}$ cannot be directly obtained for k = 1 and 5; thus, their values are empirically estimated using a type of inversion technique based on Eq. (3) and CONTRAIL data for the ExUTLS (Sawa et al., 2015). If the i-th CONTRAIL datum is obtained at the spatiotemporal point $(\emptyset_{eqC(i)}, \theta_{C(i)}, \mathcal{M}_{C(i)})$, the mixing ratio for species S ($\equiv X^S_{C(i)}$) and the values

Atmos. Chem. Phys. Discuss., https://doi.org/10.5194/acp-2018-1030
Manuscript under review for journal Atmos. Chem. Phys.
Discussion started: 26 November 2018

reconstructed for S are interpolated to the same point (=$X^S(\emptyset_{eqC(i)}, \theta_{C(i)}, \mathcal{M}_{C(i)})$). The summation of square differences (SD_{sum}) between the two is calculated as

$$SD_{sum} = \sum_{i=1}^{N_{Cmax}} \left\{ X^S_{C(i)}\left(\emptyset_{eqC(i)}, \theta_{C(i)}, \mathcal{M}_{C(i)}\right) - X^S(\emptyset_{eqC(i)}, \theta_{C(i)}, \mathcal{M}_{C(i)}) \right\}^2, \quad (4)$$

where N_{Cmax} denotes the total number of CONTRAIL measurements used; $X^S{}_{ORG_1}$ and $X^S{}_{ORG_5}$ are obtained as values that minimize SD_{sum} for each target month ($\mathcal{M}_{target}$) by combining the variables for 4 months ($\mathcal{M}_{target} - 3$ to $\mathcal{M}_{target}$). In this estimation, X^S in Eq. (4) reconstructed for each combination is affected not only by the employed $X^S{}_{ORG_1}(\mathcal{M}_{target})$ and $X^S{}_{ORG_5}(\mathcal{M}_{target})$, but also by their values for specific months from $\mathcal{M}_{target} - 3$ to $\mathcal{M}_{target} - 1$, because trajectories extend to a maximum of 90 days in this study. Therefore, this procedure is repeated over a whole year by sequentially changing the target month until both $X^S{}_{ORG_1}$ and $X^S{}_{ORG_5}$ are unchanged and minimize SD_{sum} for all months.

Because this study performs a trajectory analysis using an objective reanalysis dataset, subgrid-scale processes, such as the sporadic injection of tropospheric air masses into the ExUTLS, cannot be explicitly reproduced. Thus, to remove the influence of such sporadic processes, CONTRAIL data with CO mixing ratios higher than 80 ppb, i.e., parts per billion by moles and hereafter the same goes ppm and ppt, in the region above 340 K and north of 60° N equivalent latitude are not used in this estimation. Thus, values obtained for $X^S{}_{ORG_1}$ and $X^S{}_{ORG_5}$ may show spurious fluctuations. To reduce these fluctuations, we take 3-month running averages of the values estimated for the two variables. The spatiotemporal distribution of S in the ExUTLS is reconstructed using Eq. (3) and $X^S{}_{ORG_k}$ (k = 1–5) values for a whole year.

3 Results

3.1 Mixing fraction

Mixing fractions were estimated as a function of $\emptyset_{eq}$, θ, and $\mathcal{M}$. Their distributions in a $\emptyset_{eq}$–θ cross-section are shown in Fig. 3 for January together with the climatology of monthly averaged potential vorticity for the period from 2012 to 2016 obtained from ERA-Interim. In winter, mixing fractions of the high-latitude stratosphere dominate regions north of 40° N and higher than 350 K in altitude. In particular, regions where the altitude and latitude are greater than 360 K and 50° N, respectively, are almost entirely occupied by stratospheric air masses, of which roughly 30 % have originated in the deep stratosphere via the deep branch of the BDC in regions where the potential vorticity exceeds ~10 PVU (Fig. 3c). However, mixing fractions of the tropical troposphere dominate regions of lower latitude and altitude where the potential vorticity is less than ~4 PVU. These mixing fractions are higher than 50 %, except in regions lower than 310 K in altitude. Air masses in regions lower than 310 K generally originate in the mid-latitude LT with mixing fractions up to ~50 %, with few air masses originating in the high-latitude LT. The remainder (i.e., UTLS air masses that are not categorized by their origins) are distributed between 4 and 8 PVU with a maximum at around 320 K at higher latitudes. The mixing fractions of the high-latitude LT are small during this season.

The mixing fractions for April are shown in Fig. 4. In spring, mixing fractions of the high-latitude stratosphere generally decrease from their winter values. In particular, the region occupied by air masses originating in the shallow branch of the BDC becomes confined to above ~355 K in altitude. At the same time, mixing fractions of the UTLS increase. The region where UTLS mixing fractions are higher than 40 % spreads down to ~40° N equivalent latitude and up to 360 K in altitude. However, high-latitude stratospheric air masses still dominate regions north of 50° N and higher than 370 K in altitude, and tropical tropospheric air masses continue to dominate regions where the potential vorticity is less than ~4 PVU, except for regions below 310 K. Mixing fractions of the high-latitude LT remain small during spring.

Estimated mixing fractions for July are shown in Fig. 5. In summer, mixing fractions of the high-latitude stratosphere become less dominant. In particular, those originating in the deep branch of the BDC (Fig. 5c) are small over the whole ExUTLS. Stratospheric air masses, almost all of which originate in the shallow branch of the BDC, are distributed in a small region above ~370 K at high latitudes. In contrast, there is expansion of the region in which the mixing fractions of the tropical troposphere are dominant. In particular, nearly 100 % of the air masses in the region above 340 K and south of 40° N originate in the tropical troposphere. Mixing fractions of the UTLS are smaller than in spring but remain at values higher than 40 % in regions where the potential vorticity is greater than ~6 PVU and the potential temperature is less than 360 K, with a maximum at around 340 K. Only during this season do mixing fractions of air masses originating in the high-latitude LT reach up to ~50 %, but these are limited to a region below ~320 K. Mixing fractions of the mid-latitude LT become smaller, but the region where they are higher than 20 % becomes wider than during spring, expanding up to 340 K at all equivalent latitudes.

Mixing fractions for October are shown in Fig. 6. During autumn, high mixing fractions of the high-latitude stratosphere broaden again in the region above 350 K. However, those originating in the deep branch of the BDC are small. Mixing fractions of the high-latitude LT are suppressed, and those of the UTLS decrease to below 40 %, except for a small region around 330 K between 70° N and 90° N. At the same time, the region where mixing fractions of the tropical troposphere are higher than 40 % becomes larger than during summer and extends up to 80° N along ~4–6 PVU potential vorticity surfaces. In the region below 320 K, mid-latitude LT air masses dominate. These seasonal results are compared with previous studies in Sect. 4.1. The robustness and limitations of our estimates are discussed in Sect. 4.3.

3.2 Original composition and AoA

As described in Sect. 2.2, detrended mixing ratios of CH_4, N_2O, CO, SF_6, and CO_2 observed in the tropical troposphere, mid-latitude LT, and high-latitude LT are assigned to their original mixing ratios for $k = 2$, 3, and 4, respectively. For $k = 1$ and 5, the original mixing ratios are estimated from mixing fractions (e.g., Figs 3–6) and CONTRAIL measurements in the ExUTLS for each month. Figure 7 shows the original mixing ratios of each species assigned to an individual trajectory according to Eq. (3). Whereas CH_4 and SF_6 show some seasonal variations and latitudinal gradients in the troposphere, N_2O does not. In contrast to the troposphere, CH_4, N_2O, and SF_6, in high-latitude stratospheric and UTLS air masses show distinct seasonal variations of similar phase, with minima in boreal spring and maxima in summer/autumn. For CO, there are large seasonal variations in high- and mid-latitude tropospheric air masses, but tropical tropospheric values show little seasonal variation. The CO mixing

ratios for the high-latitude stratosphere and UTLS show seasonal variability (they may be analytical artefacts), but are less than 50 and 70 ppb throughout the year, respectively. For CO_2, seasonal variations are largest in the high-latitude troposphere; mixing ratios in the tropical troposphere, high-latitude stratosphere, and UTLS show seasonal variations, but with differing phases.

The AoA of the stratospheric and UTLS air masses estimated from 10-year trajectories are shown in Fig. 7f. Stratospheric air masses transported via the deep branch of the BDC have AoA exceeding 5.5 years, whereas those transported via the shallow branch have AoA of ~1 year. The average AoA among air masses originating in both branches shows a seasonal variation, with maximum values of ~2.5 years in March and minimum values of ~1.4 years in August. The AoA of UTLS air masses also shows a seasonal variation, with a maximum in boreal summer and minimum in winter. The relationship between the original composition of stratospheric air masses and their AoA is discussed in Sect. 4.2.

3.3 Reconstructions

Chemical distributions reconstructed from the mixing fractions of air masses (Sect. 3.1) and their original compositions (Sect. 3.2) are shown for January (Fig. 8) together with observation results obtained from CONTRAIL measurements over Siberia and monthly averaged potential vorticity obtained from the ERA-Interim dataset during the period from 2012 to 2016. Spatial distributions of all chemical species generally show higher mixing ratios with decreasing potential temperature, equivalent latitude, or potential vorticity. Conversely, the distribution of AoA generally shows a higher age with increasing potential temperature, equivalent latitude, or potential vorticity. In particular, an AoA of greater than 3 years is estimated in the deep ExUTLS for regions higher than 390 K and north of 75° N.

The reconstructions and AoA for April (Fig. 9) show spatial distributions of CH_4, N_2O, and SF_6 mixing ratios that generally increase with decreasing potential temperature, equivalent latitude, or potential vorticity, whereas those of CO and CO_2 have minima near 370 K north of 50° N equivalent latitude. Although the minimum for CO may be an artefact of the reconstruction procedure, its magnitude is less than 10 ppb, which is significantly smaller than the seasonal variation. Thus, it is not expected to have an influence on the seasonal-characteristic results. The minimum for CO_2 may be considered part of the "tape recorder" of CO_2 mixing ratios in the UTLS (Andrews et al., 1999). The AoA distribution has a structure similar to that shown for January; i.e., age that increases with potential temperature, equivalent latitude, or potential vorticity.

The spatial distributions of the chemical species and AoA change more during summer than during winter and spring (Fig. 10). In particular, those of CH_4 and N_2O show minima at around 370 K at high equivalent latitudes, similar to those of CO_2 during April (Fig. 9e). They may be formed by remainder of the high-latitude stratospheric air masses which were transported during spring when CH_4 and N_2O mixing ratios ware small. However, those of SF_6 do not show such minima in the ExUTLS region. For CO_2, the minimum descends to around 345 K potential temperature, and some CONTRAIL measurements show significantly lower mixing ratios than the reconstructed values. The difference between the CONTRAIL measurements and the reconstructions will be discussed in the last part of this section. The AoA becomes significantly smaller during this season

compared with winter and spring. In particular, the AoA of nearly the entire region with potential vorticity of <8 PVU is less than 1 year.

In autumn, the chemical gradients for CH_4, N_2O, SF_6, and CO_2 in the ExUTLS are reduced (Fig. 11), in large part because CH_4 and N_2O mixing ratios in the deeper ExUTLS increase up to 1750 ppb for CH_4 and 315 ppb for N_2O. The reconstructed CO_2 mixing ratios show a nearly homogeneous distribution in the ExUTLS. The spatial distribution of CO, however, retains a steep gradient, because its chemical lifetime is small (a few months). The distribution of AoA during this season is similar to that during summer, with the AoA of nearly the entire region with potential vorticity of <8 PVU being less than 1 year.

Reconstructions for CH_4, N_2O, CO, SF_6, and CO_2 are compared with CONTRAIL measurements after spatial interpolation to each measurement point for each month (Fig. 12). The reconstructions generally agree with the measurements, with some outliers during the summer season. In particular, some observed CO_2 mixing ratios have much smaller values than the reconstructions during boreal summer (Fig. 12e). This may be caused by CO_2 absorption by the local Eurasian forest and enhanced subgrid-scale vertical transport by local convection during the summer season. Figure 12f shows the relationship between AoA estimated from the 10-year trajectory analysis and SF_6 observed by CONTRAIL. Results of the analysis show a negative correlation with a fit-line of slope −0.33 ppt/year, which is the inverse of the increasing trend of SF_6 measured at Mauna Loa. This means that our AoA estimates agree well with other AoA estimates based on SF_6 mixing ratios and their trend in the troposphere (e.g., Sawa et al., 2015). Thus, SF_6 decreases with increasing AoA at a rate equal to the sign-reversed increasing trend of background SF_6, thereby supporting the robustness of our AoA estimates.

4 Discussion

One goal of the current study is to visualize how seasonal variations in dynamical and chemical transport affect the spatiotemporal distributions of chemical species in the ExUTLS. This is accomplished by determining the seasonal characteristics of mixing fractions of ExUTLS air masses originating in each region k at fixed points with those of the reconstructions for each species, and comparing the distribution of each species in the ExUTLS with the original mixing fraction in each origin region. We next discuss the results of this analysis, together with the limitations of the current study.

4.1 Seasonal characteristics of dynamical and chemical transport

To identify the characteristics of seasonal variations in mixing fractions and reconstructions at fixed locations, four regions are selected: mid-latitude upper ExUTLS (45° N, 370 K), high-latitude upper ExUTLS (75° N, 370 K), mid-latitude lower ExUTLS (45° N, 320 K), and high-latitude lower ExUTLS (75° N, 320 K). Figure 13 shows seasonal variations in the mixing fractions of each origin evaluated at the four locations. In the mid-latitude upper ExUTLS, mixing fractions of the tropical troposphere become high, exceeding 40 % during summer and autumn. This increase may be related to the Asian summer monsoon according to confirmation of the trajectories. In the other seasons, mixing fractions of the high-latitude stratosphere dominate. In particular, those that travelled via the shallow branch of the BDC exceed 50 %. The mixing fractions of the mid-

and high-latitude LT are nearly zero throughout the year. In the high-latitude upper ExUTLS, mixing fractions of the high-latitude stratosphere dominate and exceed 60 % throughout the year. Furthermore, mixing fractions of air masses that travelled via the deep branch of the BDC exceed 20 % during the period from January to April, whereas tropical tropospheric air masses generally fail to reach this region during this period. In the mid-latitude lower ExUTLS, tropospheric mixing fractions are dominant. In particular, those of the mid-latitude troposphere exceed 40 % during summer and those of the high-latitude troposphere exceed 20 % during July and August. During winter, however, tropical tropospheric air masses dominate. In the high-latitude lower ExUTLS, mixing fractions of the mid- and high-latitude LT are enhanced but their fractions are lower than those of the mid-latitude lower ExUTLS. In winter, mixing fractions of the tropical troposphere and high-latitude stratosphere are roughly 20 %, whereas those of the UTLS achieve the highest value, with a maximum exceeding 60 % in March.

In addition to seasonal variation in the mixing fractions, that in the composition of the original air masses (Fig. 7) also contribute to seasonal variations in the chemical distributions in the ExUTLS. Figure 14 reveals that seasonal variations in the reconstructions for each species and the trajectory-estimated AoA in each of the four locations follow the same patterns as shown in Fig. 13. Note that the CONTRAIL data are plotted if the measurement was conducted within ±5° in equivalent latitude and within ±5 K in potential temperature of one of the four locations. This results in few plotted CONTRAIL observations in mid- and high-latitude lower ExUTLS regions during summer, and no observations in mid- and high-latitude upper ExUTLS regions from June to January. This is caused by the seasonality of the thermal and dynamical structures of the ExUTLS and fixed flight altitudes. Despite the sparse and non-uniform observational field, the spatiotemporal distributions of chemical species, together with the mixing fractions of the original air masses, can be resolved. This ability is one of the important advantages of the current analysis. The mixing ratios of CH_4 and N_2O shown modest seasonal variations in the lower ExUTLS, whereas they show large seasonal variations in the upper ExUTLS, with minima in spring and maxima in autumn. The minima in spring are due to the transport of stratospheric air masses, which have low CH_4 and N_2O mixing ratios during this season (Fig. 7). This seasonal variation in chemical abundance for stratospheric air masses is discussed further in the next section. In contrast to CH_4 and N_2O, CO mixing ratios show smaller seasonal variations in the upper ExUTLS than in the lower ExUTLS. This can be explained by the transport of mid-latitude LT air masses, which have higher CO mixing ratios than the other air masses, to the lower ExUTLS during summer. The seasonal characteristics of SF_6 mixing ratios are similar to those of CH_4 and N_2O. In particular, the phase of seasonal variations in the upper ExUTLS is synchronized with those of CH_4 and N_2O, whereas the relative amplitude of seasonal variations in the lower ExUTLS is somewhat smaller. The difference of amplitudes in the upper ExUTLS among SF_6, CH_4, and N_2O is likely caused by the presence or absence of sinks for these species in the stratosphere, as discussed further in the next section. The phase of seasonal variations of CO_2 mixing ratios in the lower ExUTLS is nearly synchronized between the mid- and high-latitudes, with the largest amplitude being evident in the mid-latitude ExUTLS. The phase of CO_2 variations in the upper ExUTLS is quite different from that in the lower ExUTLS, with maxima during summer. This seasonal variation in the upper ExUTLS is consistent with observational estimates by Strahan et al. (2007).

Seasonal variations in AoA evaluated at the four locations are shown in Fig. 14f. The phase of seasonal variations for the four locations is roughly synchronized, whereas the absolute values are clearly different. For example, AoA in the high-latitude upper ExUTLS has a maximum of more than 2.5 years during spring and a minimum of ~1 year during the end of summer, whereas in the mid-latitude lower ExUTLS the maximum is only ~0.4 years and occurs during the period from winter to spring. The amplitude of AoA variations in the ExUTLS is likely related to air-mass mixing from the high-latitude stratosphere, especially when this involves air masses that have been transported via the deep branch of the BDC. This point is discussed further in the next section, in relation to seasonal variations in chemical composition.

4.2 Original compositions and mixing effects

As discussed in the previous section, the distributions of CO and CO_2 in the ExUTLS are strongly affected by tropospheric air masses because CO has a short chemical lifetime and CO_2 shows large seasonal variations in the high- and mid-latitude LT. For CH_4, N_2O, and SF_6, however, seasonal variations in mixing fractions of the stratospheric air masses and in the compositions of the original air masses are considered to be essential factors in their spatiotemporal distributions in the ExUTLS. Here, we discuss seasonal variations in the composition of stratospheric air masses and how this affects chemical distributions via mixing with tropospheric air masses in the ExUTLS. Figure 15 shows the relationships between chemical abundances from CONTRAIL measurements and the AoA estimated from the trajectories and interpolated to each CONTRAIL measurement location (i.e., $\emptyset_{eqC(i)}$, $\theta_{C(i)}$, and $\mathcal{M}_{C(i)}$ in Sect. 2.2), along with these relationships for each original air mass. The AoA for stratospheric air masses are the same as those shown in Fig. 7f, whereas the AoA for the tropical, mid- and high-latitude troposphere are set to zero. Thus, the denotations for the tropospheric air masses only move vertically in the cross-sections according to their seasonal variations. Overall, the CONTRAIL measurements are roughly distributed on lines connecting the tropospheric and stratospheric air masses for all seasons and chemical compositions. This linear distribution suggests that dynamical mixing of tropospheric with stratospheric air masses shapes the chemical distributions of the ExUTLS. A comparison of the distribution of CONTRAIL measurements with trends in the troposphere for SF_6 and CO_2 shows that the CONTRAIL measurements are distributed along the lines of the sign-reversed trends, whereas for CH_4 and N_2O, measurements depart from the lines of the sign-reversed trends toward lower mixing ratios with increasing AoA. This deflection can be interpreted as being due to their stratospheric sinks; i.e., the photo-chemical destruction of CH_4 and N_2O in the stratosphere, with no such destruction of SF_6 and CO_2.

Both the AoA and chemical abundance of the original air masses from the high-latitude stratosphere show seasonal variations that might be caused by seasonal variations in mass fluxes from the deep and shallow branches of the BDC. Figure 15f shows seasonal variations in AoA and integrated PDF from 0 to 10 years for air masses originating in the high-latitude stratosphere as well as those separately evaluated for air masses that have travelled via the deep and shallow branches of the BDC. As the PDF is calculated with a weighting factor according to area and density, as in Eq. (1), their integrations reveal relative masses. Air masses originating in the shallow branch have a minimum in July and maximum in December, whereas the deep branch has a minimum in September and maximum in March. These phase-lagged seasonal variations cause seasonal variations in the

total mixing fractions of the high-latitude stratosphere and its averaged AoA, as well as the minima of CH_4, N_2O, and SF_6 mixing ratios in spring. For example, we estimate 315 ppb N_2O and 1.4 years AoA in autumn, and 280 ppb and 2.3 years, respectively, in spring. This relationship between the decrease in N_2O from its tropospheric value and the AoA is consistent with those presented by Volk et al. (1997) and Andrews et al. (2001). If we assume that the N_2O destruction rate along its path through the shallow branch is negligibly small compared with that through the deep branch, the differences between the sign-reversed trend (dashed line in Fig. 15b) and the observed N_2O mixing ratios (small filled circles in Fig. 15b) or those estimated for the original high-latitude stratospheric air masses (open circles in Fig. 15b) reflect the contribution of mixing with air masses coming from the deep branch of the BDC. The current study estimates approximately 25 % and 10 % of air masses following the deep branch are of stratospheric origin in spring and autumn, respectively, and the AoA is estimated to be ~5.5 years (Fig. 15f). Andrews et al. (2001) estimated the N_2O mixing ratio to be ~80 ppb in the mid-latitude deep stratosphere where the AoA is estimated to be 5.5 years from the CO_2 mixing ratio. As their estimates are normalized to 1997 tropospheric values, the quantitative difference in the baseline N_2O mixing ratios may differ by ~20 ppb from the present values. If we assume the N_2O mixing ratio of air masses originating in the deep branch of the BDC is 100 ppb, and that air masses are mixed at ratios of 25 % and 10 % with air masses whose N_2O mixing ratio is 330 ppb, such mixing leads to ~270 ppb and ~310 ppb N_2O mixing ratios, respectively. These values generally agree with the N_2O mixing ratios of ~280 ppb in April and ~315 ppb in October estimated for the original stratospheric air masses shown in Fig. 7b.

The same arguments are valid for CH_4 with respect to the relationship between stratospheric CH_4 mixing ratios and AoA; i.e., ~600 ppb in regions where the AoA is 5.5 years, as estimated by Röckmann et al. (2011). Thus, the relationship between AoA and mixing ratios of N_2O and CH_4 in the ExUTLS, which changes with the season, is driven by seasonal variations in air masses transported via the shallow and deep branches of the BDC and by the mixing of such stratospheric air masses with tropospheric air masses in the ExUTLS.

4.3 Limitations of the current study

This study provides a detailed explanation of seasonal variations in chemical distributions and transport in the ExUTLS from a dynamical standpoint using trajectory analysis in combination with aircraft measurements. Results suggest that the spatiotemporal distributions of CH_4, N_2O, SF_6, and AoA in the ExUTLS are controlled primarily by air-mass transport via the deep and shallow branches of the BDC and by their mixing with tropospheric air masses in the ExUTLS, whereas those of CO and CO_2 are controlled largely by the tropospheric air masses, because CO has a short chemical lifetime and CO_2 shows large seasonal variations in the mid-latitude LT. However, some assumptions and limitations of the current study should be mentioned.

First, some uncertainty results from the use of ERA-Interim data in trajectory analyses. Trajectory results generally depend on the resolution of the input data. We performed sensitivity analyses to clarify this dependency in our mixing fraction estimates (Appendix A). Results confirm that our estimates are independent of the resolution of the ERA-Interim data, at least as they relate to statistical characteristics. Furthermore, it is known that AoA calculated from trajectory analyses using ERA-Interim

data are somewhat young-biased. For example, these estimated AoA values are ~30 % younger than those estimated from balloon-borne observations in the middle stratosphere, as demonstrated by Inai (2018). To address this issue, trajectory-based AoA values are uniformly corrected by a correction factor of 1.43 in this study. There is, however, a possibility that the bias differs with the meteorological region, because different mechanisms drive the shallow and deep branches of the BDC (e.g., Birner and Bönisch, 2011). In addition, to estimate mean AoA from an age spectrum with finite time lengths (e.g., the 10 years used in this study), a tail correction is required. Though this study does not employ a tail correction, the required correction is estimated to be less than 5 % by Inai (2018) and approximately 10 % by Ploeger and Birner (2016). Thus, it is smaller than the correction factor used here. Most importantly, AoA estimates used in this study agree well with those expected from observed SF_6 mixing ratios.

The second limitation is related to the criteria for the determination of air-mass origin. These criteria might strongly affect mixing-fraction estimates and are thus expected to contribute to the uncertainty of this analysis, to some degree. A comprehensive sensitivity test to address this issue, focusing on in-mixing in the TTL, has been reported by Inai (2018), who found that the mixing fraction can vary by 40 % to 180 %, depending on the choice of criteria. Though the same test could be applied to the current study, the estimated mixing-fraction distributions are comparable to those estimated by Umezawa et al. (2015). Moreover, these estimates are indirectly validated by the CONTRAIL observations, through the reconstruction of the chemical distributions (as evident in Figs 8–11). This agreement supports our criteria selection and suggests that our estimated mixing fractions are not, at least, grossly wrong.

Another limitation may arise from the analysis methodology. The observed mixing ratios of CH_4, N_2O, CO, SF_6, and CO_2 are used after removing linear trends for each time-series, and are considered to be a function of month. This treatment decreases the precision of observations if the observed values have non-liner interannual variations. Furthermore, the CONTRAIL measurements were conducted once a month. Thus, one observed value represents atmospheric conditions at a specific spatiotemporal point, whereas the analysis field has a coarser spatiotemporal resolution, corresponding to, at minimum, that of the grid scale in ERA-Interim dataset. Such a mismatch in spatiotemporal resolution may contribute to the lack of agreement between the reconstructions and CONTRAIL measurements during summer (Fig. 10e). However, uncertainties arising from these issues are minimized by the use of equivalent latitude and potential temperature, which are dynamically conserved quantities. Though the current study covers only the ExUTLS over a longitudinal range from 0° E to 140° E for comparison with the CONTRAIL measurements, the mixing fractions and reconstructions are trial-evaluated over Europe and North America (Appendix A). Results confirm that the mixing fractions are consistent between the two regions, and thus support the robustness of the current study.

5 Summary

To identify the origin of air masses in the ExUTLS, kinematic backward trajectories were calculated for 90 days following the method of Inai (2018) using ECMWF ERA-Interim data as input. The analysis period extends from January 2012 to December

2016, and trajectories were categorized by origins in the high-latitude stratosphere, tropical troposphere, mid-latitude LT, high-latitude LT, and unclassified regions (UTLS) based on meteorological parameters along each individual trajectory. The mixing fractions of air masses originating in each region were estimated as a function of equivalent latitude, potential temperature, and month. Furthermore, using a 10-year trajectory, the mixing fractions of air masses originating via the shallow and deep branches of the BDC were separately estimated along with the AoA.

The mixing fractions show obvious seasonal variations. In the mid-latitude upper ExUTLS, mixing fractions of the tropical troposphere exceed 40 % during boreal summer and autumn in association with the Asian summer monsoon, whereas mixing fractions of the high-latitude stratosphere via the shallow branch of the BDC are dominant during winter and spring. In the high-latitude upper ExUTLS, mixing fractions of the high-latitude stratosphere exceed 60 % throughout the year. In the lower ExUTLS, mixing fractions of the mid- and high-latitude troposphere are large during summer, while during winter, mixing fractions of the tropical troposphere and UTLS are dominant in the mid- and high-latitude lower ExUTLS, respectively.

By incorporating the time-series of mixing ratios for several chemical species obtained from ground-based and air-borne observations into the estimated mixing fractions, the spatiotemporal distributions of the chemical species CH_4, N_2O, CO, SF_6, and CO_2 in the ExUTLS were reconstructed, along with estimations of the original composition of the stratospheric and UTLS air masses. The reconstructions agree well with CONTRAIL measurements in the ExUTLS. Furthermore, uniform spatiotemporal species distributions are obtained for the ExUTLS from non-uniform observations. The mixing fractions and AoA of each reconstruction are discussed. Distributions of CO and CO_2 are strongly affected by tropospheric air masses because of the short chemical lifetime of the former and large seasonal variations in the troposphere of the latter. In contrast, CH_4, N_2O, and SF_6 distributions are controlled primarily by seasonal variations in air masses transported from the stratosphere, and in particular those transported via the deep branch of the BDC for CH_4 and N_2O. This interpretation is qualitatively and quantitatively consistent with the spatiotemporal AoA distributions.

This study developed and demonstrated a unique and effective method to exploit the advantages of observational data in combination with trajectory analysis. This method provides a means to understand both dynamical transport and chemical distribution from a new perspective. Furthermore, this technique can be applied to other data (e.g., species isotope ratios) or analyses of regions where trajectory calculations keep their effectiveness.

Appendix A. Sensitivity analyses

It is well known that results from trajectory analyses are affected by the resolution of input meteorological data. For example, Inai (2018) suggests that the mixing fraction of stratospheric air masses in the upper TTL can vary by ~50 % in magnitude. Here, the sensitivity of our results to data resolution is tested. Figure A1 shows the dependence of mixing fractions on the resolution of meteorological data for trajectories launched each month. Mixing fractions calculated from ERA-Interim data and used in this study (0.75° × 0.75° horizontal resolution, 60 vertical levels) are compared with those using a coarser resolution

(1.5° × 1.5° horizontal resolution, 37 vertical levels). Mixing fractions were evaluated for each bin set in an equivalent latitude–potential temperature cross-section (crosses). Results confirm that these points are distributed in a linear fashion with slopes of around 1.0 regardless of season. This suggests that the mixing fractions are not quantitatively or qualitatively dependent on the resolution of the input data. This independence differs from the findings of Inai (2018), possibly because transport mechanisms in the ExUTLS are related to synoptic-scale mechanisms rather than convective activity, which dominates the tropical region.

In the current study, mixing fractions were estimated only for the longitudinal region between 0° E and 140° E, selected for comparison with CONTRAIL measurements over Siberia. Previous studies have investigated mixing processes between tropospheric and stratospheric air masses over different longitudinal regions; e.g., over North America (Pan et al., 2010). To compare our results with these studies, the dependence of mixing fraction on longitudinal region was tested. Figure A2 compares mixing fractions evaluated over Siberia and North America. Results confirm that the data points in Fig. A2 (crosses) are distributed in a linear fashion with slopes of around 1.0 regardless of season. This suggests that the mixing fractions are not quantitatively and qualitatively dependent on longitudinal region. This independence may arise from the employment of equivalent latitude and potential temperature, which are dynamically conserved parameters, in this analysis.

Author contribution

Yoichi Inai designed the study and carried it out. Toshinobu Machida, Hidekazu Matsueda, Yousuke Sawa, Kazuhiro Tsuboi, Keiichi Katsumata obtained the measurement data and Shinji Morimoto, Shuji Aoki, Takakiyo Nakazawa developed the measurement system. Yoichi Inai and Ryo Fujita prepared the manuscript with contributions from all co-authors.

Acknowledgements

The authors would like to acknowledge the support of many engineers from Japan Airlines and JAMCO Tokyo. All trace-gas mixing-ratio data at ground-based sites were provided by NOAA/ESRL (National Oceanic and Atmospheric Administration/Earth System Research Laboratory) and were downloaded from the WMO/WDCGG website (https://gaw.kishou.go.jp/). This work was supported by Grants-in-Aid for Scientific Research (18K03738 and 26220101) from the Japan Society for the Promotion of Science and the Arctic Challenge for Sustainability (ArCS) Project by the Ministry of Education, Culture, Sports, Science and Technology, Japan. We thank Masashi Kohma for valuable discussion. We also thank ECMWF for providing the ERA-Interim data. All figures were produced using the GFD-DENNOU Library.

References

Andersson, S., Martinsson, B., Vernier, J.-P., Friberg, J., Brenninkmeijer, C., Hermann, M., Velthoven, M., and Zahn, A.: Significant radiative impact of volcanic aerosol in the lowermost stratosphere, Nat. Commun., 6, 7692, doi:10.1038/ncomms8692, 2015.

Andrews, A. E., Boering, K. A., Daube, B. C., Wofsy, S. C., Hintsha, E. J., Weinstock, E. M., and Bui, T. P.: Empirical age spectra for the lower tropical stratosphere from in sitiu observations of CO_2: implications for stratospheric transport, J. Geophys. Res., 104, 26581–26596, 1999.

Andrews, A. E., Boering, K. A., Daube, B. C., Wofsy, S. C., Loewenstein, M., Jost, H., Podolske, J. R., Webster, C. R., Herman, R. L., Scott, D. C., Flesch, G. J., Moyer, E. J., Elkins, J. W., Dutton, G. S., Hurst, D. F., Moore, F. L., Ray, E. A., Romashkin, P. A., and Strahan, S. E.: Mean ages of stratospheric air derived from in situ observations of CO_2, CH_4, and N_2O, J. Geophys. Res., 106, 32295–32314, doi:10.1029/2001JD000465, 2001.

Appenzeller, C., Holton, J. R., and Rosenlof, K. H.: Seasonal variation of mass transport across the tropopause. J. Geophys. Res. 101, 15071–15078, 1996.

Birner, T., and Bönisch, H.: Residual circulation trajectories and transit times into the extratropical lowermost stratosphere, Atmos. Chem. Phys., 11, 817–827, doi:10.5194/acp-11-817-2011, 2011.

Bönisch, H., Engel, A., Curtius, J., Birner, Th., and Hoor, P.: Quantifying transport into the lowermost stratosphere using simultaneous in-situ measurements of SF_6 and CO_2, Atmos. Chem. Phys., 9, 5905-5919, https://doi.org/10.5194/acp-9-5905-2009, 2009.

Boothe, A. C. and Homeyer C. R.: Global large-scale stratosphere-troposphere exchange in modern reanalyses, Atmos. Chem. Phys., 17, 5537-5559, doi:10.5194/acp-17-5537-2017, 2017.

Brewer, A. W.: Evidence for a world circulation provided by the measurements of helium and water vapour distribution in the stratosphere, Q. J. Roy. Meteor. Soc., 75, 351–363, doi:10.1002/qj.49707532603, 1949.

Dee, D. P., Uppala, S. M., Simmons, A. J., Berrisford, P., Poli, P., Kobayashi, S., et al.: The ERA-Interim reanalysis: Configuration and performance of the data assimilation system. Quarterly Journal of the Royal Meteorological Society, 137(656), 553–597. https://doi.org/10.1002/qj.828, 2011.

Dlugokencky, E. J., Crotwell, A. M., Lang, P. M., Mund, J. W., and, Rhodes, M. E.: Atmospheric Methane Dry Air Mole Fractions from quasi-continuous measurements at Barrow, Alaska and Mauna Loa, Hawaii, 1986-2017, Version: 2018-03-19, Path: ftp://aftp.cmdl.noaa.gov/data/trace_gases/ch4/in-situ/surface/, 2018a.

Dlugokencky, E. J., Lang, P. M., Crotwell, A. M., Mund, J. W., Crotwell, M. J., and Thoning, K. W.: Atmospheric Methane Dry Air Mole Fractions from the NOAA ESRL Carbon Cycle Cooperative Global Air Sampling Network, 1983-2017, Version: 2018-08-01, Path: ftp://aftp.cmdl.noaa.gov/data/trace_gases/ch4/flask/surface/, 2018b.

Dlugokencky, E. J., Lang, P. M., Mund, J. W., Crotwell, A. M., Crotwell, M. J., and Thoning, K. W.: Atmospheric Carbon Dioxide Dry Air Mole Fractions from the NOAA ESRL Carbon Cycle Cooperative Global Air Sampling Network, 1968-2017, Version: 2018-07-31, Path: ftp://aftp.cmdl.noaa.gov/data/trace_gases/co2/flask/surface/, 2018c.

Dobson, G. M. B.: Origin and Distribution of the Polyatomic Molecules in the Atmosphere, P. Roy. Soc. Lond. A. Mat., 236, 187–193, 1956.

Gettelman, A., Hoor, P., Pan, L. L., Randel, W. J., Hegglin, M. I., and Birner, T.: The extratropical upper troposphere and lower stratosphere, Rev. Geophys., 49, RG3003, doi:10.1029/2011RG000355, 2011.

Holton, J. R. et al.: Stratosphere-troposphere exchange, Rev. Geophys., 33, 403-440, 1995.

Inai, Y.: Long-term variation in the mixing fraction of tropospheric and stratospheric air masses in the upper tropical tropopause layer. Journal of Geophysical Research: Atmospheres, 123, https://doi.org/10.1029/2018JD028300, 2018.

Ishijima, K., Nakazawa, T., Sugawara, S., Aoki, S., and Saeki, T.: Concentration variations of tropospheric nitrous oxide over Japan, Geophys. Res. Lett., 28, 171–174, doi:10.1029/2000GL011465, doi:10.1029/2000GL011465, 2001.

Lin, P., Ming, Y. and Ramaswamy, V.: Tropical climate change control of the lower stratospheric circulation, Geophys. Res. Lett., 42, 941–948, doi:10.1002/2014GL062823, 2015.

Manney, G. L., et al.: Jet characterization in the upper troposphere/lower stratosphere (UTLS): Applications to climatology and transport studies, Atmos. Chem. Phys., 11, 6115-6137, 2011.

Machida, T., Matsueda, H., Sawa, Y., Nakagawa, Y., Hirotani, K., Kondo, N., Goto, K., Nakazawa, T., Ishikawa, K., and Ogawa, T.: Worldwide measurements of atmospheric CO2 and other trace gas species using commercial airlines, J. Atmos. Oceanic Technol., 25(10), 1744–1754, doi:10.1175/2008JTECHA1082.1, 2008.

Matsueda, H., and Inoue, H. Y., Measurements of atmospheric CO2 and CH4 using a commercial airliner from 1993 to 1994, Atmos. Environ., 30, 1647–1655, 1996.

Matsueda, H., Inoue, H. Y., and Ishii, M.: Aircraft observation of carbon dioxide at 8–13 km altitude over the western Pacific from1993 to 1999, Tellus Ser. B, 54, 1–21, 2002.

Nakazawa, T., Morimoto, S., Aoki, S., and Tanaka, M.: Time and space variations of the carbon isotopic ratio of tropospheric carbon dioxide over Japan, Tellus B, 45, 258–274, 1993.

Pan, L. L., Bowman, K. P., Atlas, E. L., Wofsy, S. C., Zhang, F., Bresch, J. F., Ridley, B. A., Pittman, J. V., Homeyer, C. R., Romashkin, P. A., and Cooper, W. A.: The Stratosphere–Troposphere Analyses of Regional Transport 2008 Experiment, B. Am. Meteorol. Soc., 91, 327–342, https://doi.org/10.1175/2009BAMS2865.1, 2010.

Petron, G., Crotwell, A.M., Lang, P. M., and Dlugokencky, E.: Atmospheric Carbon Monoxide Dry Air Mole Fractions from the NOAA ESRL Carbon Cycle Cooperative Global Air Sampling Network, 1988-2017, Version: 2018-10-17, Path: ftp://aftp.cmdl.noaa.gov/data/trace_gases/co/flask/surface/, 2018.

Ploeger, F., Konopka, P., Walker, K., and Riese, M.: Quantifying pollution transport from the Asian monsoon anticyclone into the lower stratosphere, Atmos. Chem. Phys., 17, 7055-7066, https://doi.org/10.5194/acp-17-7055-2017, 2017.

Randel, W. J. and Park, M.: Deep convective influence on the Asian summer monsoon anticyclone and associated tracer variability observed with Atmospheric Infrared Sounder (AIRS), J. Geophys. Res., 111, D12314, doi:10.1029/2005JD006490, 2006.

Randel, W. J., Park, M., Emmons, L., Kinnison, D., Bernath, P., Walker, K. A., Boone, C., and Pumphrey, H.: Asian Monsoon Transport of Pollution to the Stratosphere, Science, 328, 611– 613, doi:10.1126/science.1182274, 2010.

Röckmann, T., Brass, M., Borchers, R., and Engel, A.: The isotopic composition of methane in the stratosphere: high-altitude balloon sample measurements, Atmos. Chem. Phys., 11, 13287-13304, https://doi.org/10.5194/acp-11-13287-2011, 2011.

Sawa, Y., Machida, T., Matsueda, H., Niwa, Y., Tsuboi, K., Murayama, S., Morimoto, S., and Aoki, S.: Seasonal changes of CO2, CH4, N2O, and SF6 in the upper troposphere/lower stratosphere over the Eurasian continent observed by commercial airliner, Geophys. Res. Lett., 42, 2001–2008, doi:10.1002/2014GL062734, 2015.

Strahan, S. E., Duncan, B. N., and Hoor, P.: Observationally derived transport diagnostics for the lowermost stratosphere and their application to the GMI chemistry and transport model, Atmos. Chem. Phys., 7, 2435-2445, https://doi.org/10.5194/acp-7-2435-2007, 2007.

Thoning, K. W., Kitzis, D. R., and Crotwell, A.: Atmospheric carbon dioxide dry air mole fractions from quasi-continuous measurements at Barrow, Alaska, Version: 2018-10, Path: http://dx.doi.org/10.7289/V5RR1W6B, 2017.

Umezawa, T., Goto, D., Aoki, S., Ishijima, K., Patra, P. K., Sugawara, S., Morimoto, S., and Nakazawa, T.: Variations of tropospheric methane over Japan during 1988–2010, Tellus B, 66, 23837, doi:10.3402/tellusb.v66.23837, 2014.

Vogel, B., et al.: Long-range transport pathways of tropospheric source gases originating in Asia into the northern lower stratosphere during the Asian monsoon season 2012, Atmos. Chem. Phys., 16, 15301-15325, https://doi.org/10.5194/acp-16-15301-2016, 2016.

Volk, C. M., Elkins, J. W., Fahey, D. W., Dutton, G. S., Gilligan, J. M., Loewenstein, M., Podolske, J. .R., Chan, K. R., and Gunson, M. R.: Evaluation of source gas lifetimes from Stratospheric observations, J. Geophys. Res., 102(D21), 25 543– 25 564, doi:10.1029/97JD02215, 1997.

Wernli, H., and Bourqui, M.: A Lagrangian ‘‘1-year climatology’’ of (deep) cross-tropopause exchange in the extratropical Northern Hemisphere, J. Geophys. Res., 107(D2), 4021, doi:10.1029/2001JD000812, 2002.

Atmos. Chem. Phys. Discuss., https://doi.org/10.5194/acp-2018-1030
Manuscript under review for journal Atmos. Chem. Phys.
Discussion started: 26 November 2018

Atmospheric Chemistry and Physics Discussions

Table 1: Criteria for determining the air mass origin. Each trajectory is categorized once it continuously satisfies one set of criteria during three continuous days along its path.

Category #	Origin	Criteria
k = 1	High-latitude stratosphere	Pot. temperature >380 K; lat. >45° N; pot. vorticity >6 PVU
k = 2	Tropical troposphere	Pot. temperature <350 K; lat. <30° N; pot. vorticity <2 PVU
k = 3	Mid-latitude LT	Z <4 km; 20° N < lat. < 45° N
k = 4	High-latitude LT	Z <4 km; lat. >45° N
k = 5	Unclassified (UTLS)	None of the above

5

Atmos. Chem. Phys. Discuss., https://doi.org/10.5194/acp-2018-1030
Manuscript under review for journal Atmos. Chem. Phys.
Discussion started: 26 November 2018

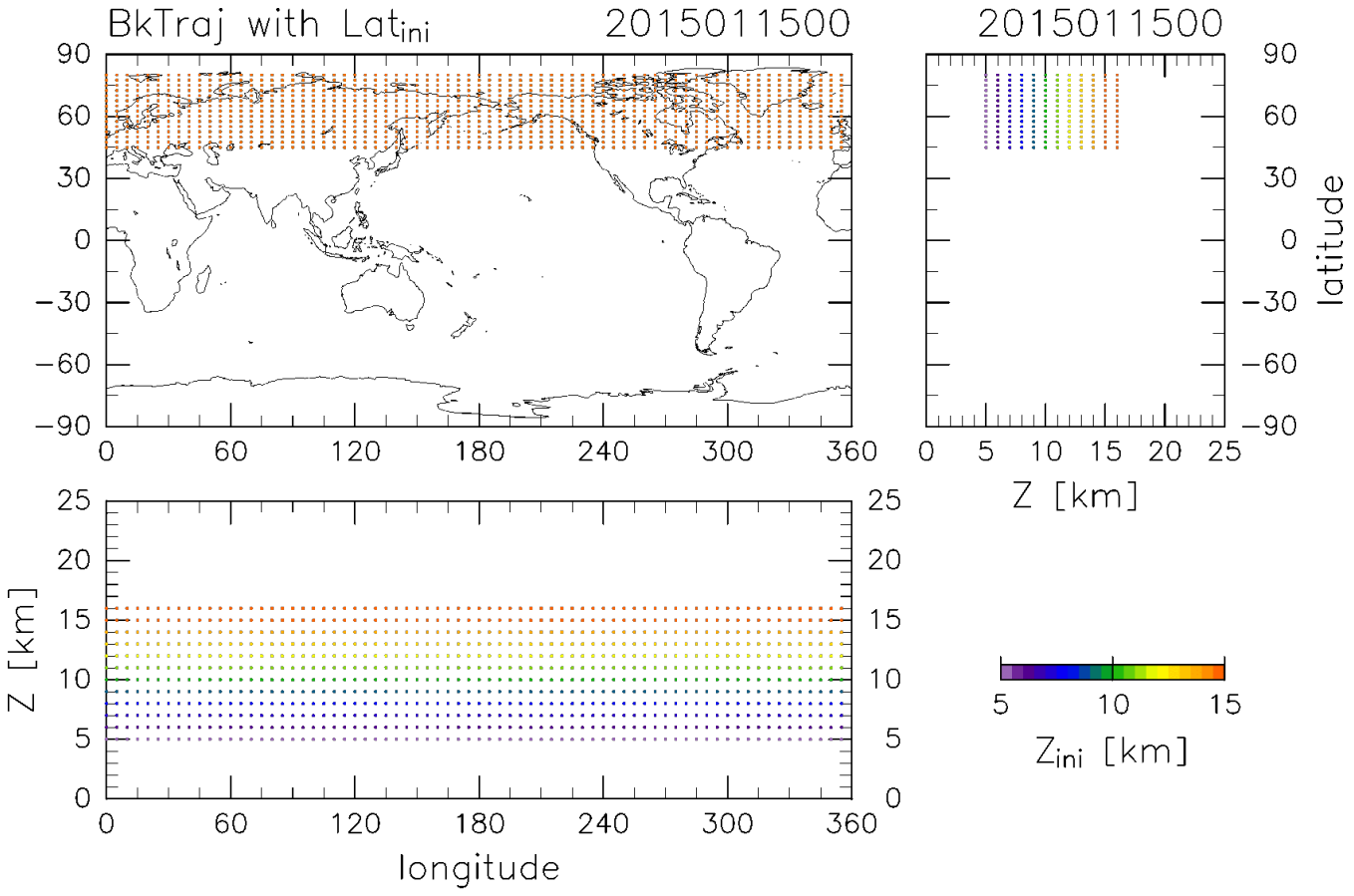

Figure 1: Initial trajectory positions projected in (top-left) longitude–latitude, (top-right) height–latitude, and (bottom) longitude–height sections. Colours indicate the initial height for each position.

Atmos. Chem. Phys. Discuss., https://doi.org/10.5194/acp-2018-1030
Manuscript under review for journal Atmos. Chem. Phys.
Discussion started: 26 November 2018

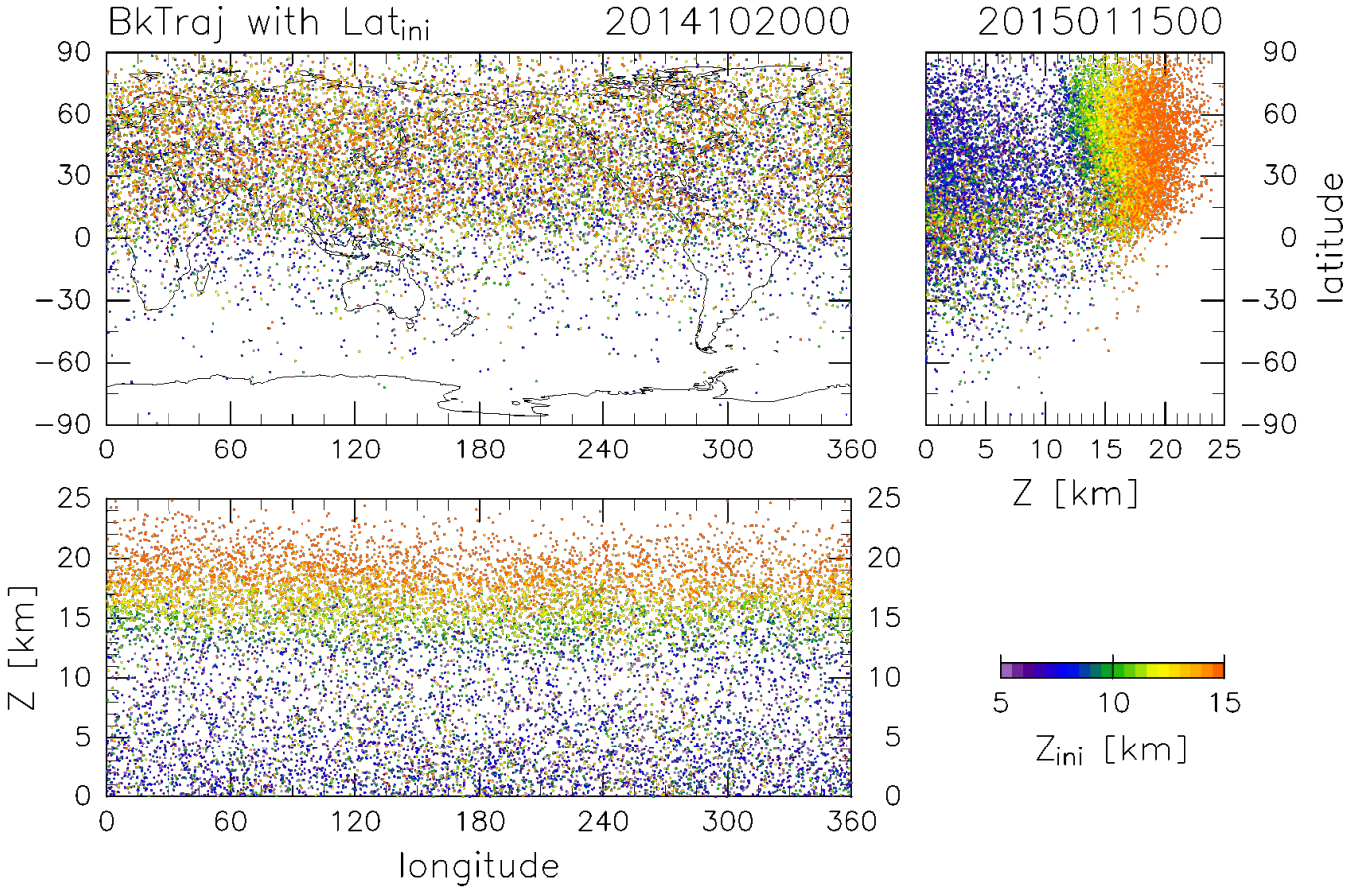

Figure 2: Same as Fig. 1, but for the terminal positions of trajectories after calculating backward for 90 days.

Atmos. Chem. Phys. Discuss., https://doi.org/10.5194/acp-2018-1030
Manuscript under review for journal Atmos. Chem. Phys.
Discussion started: 26 November 2018

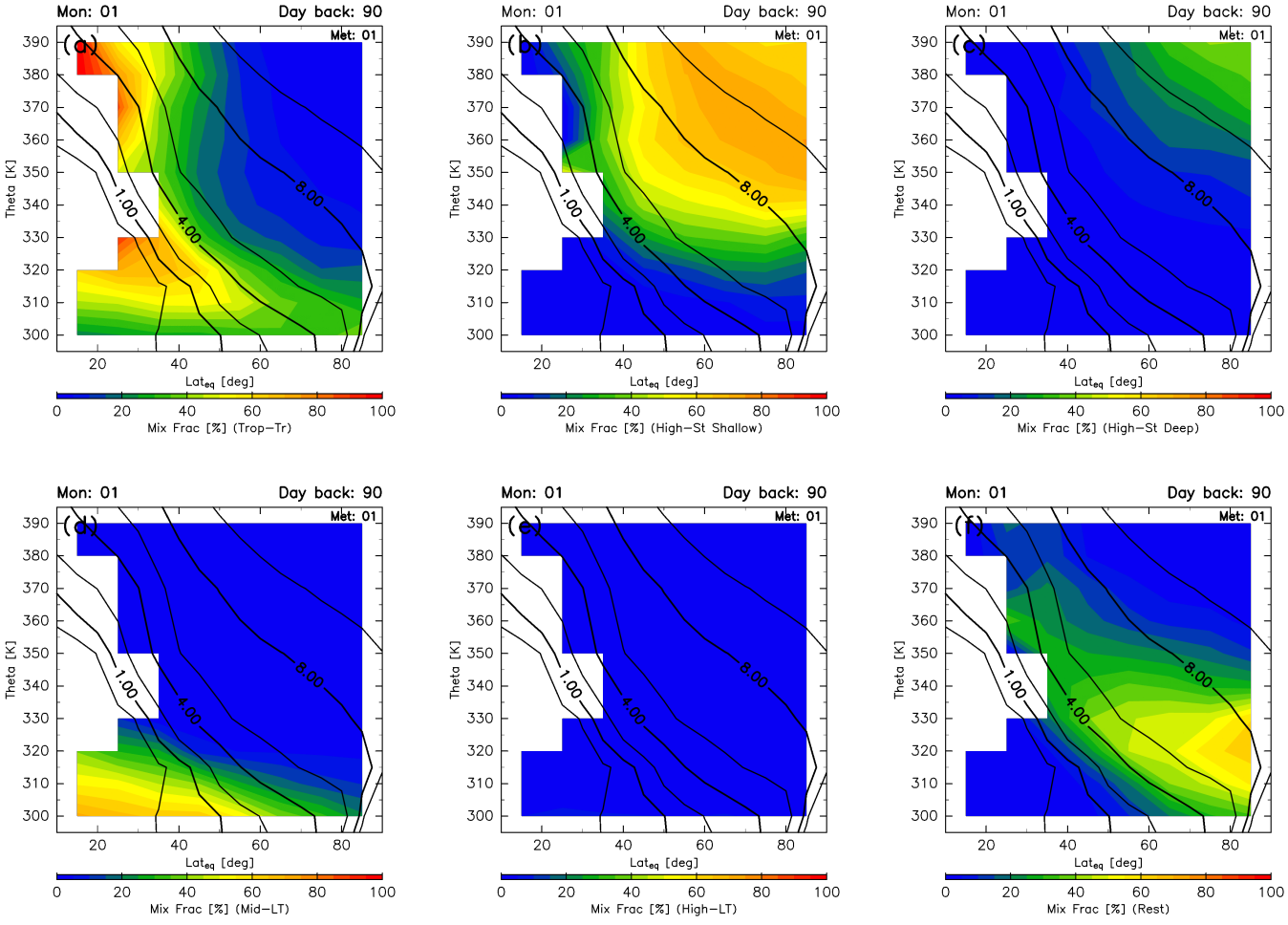

Figure 3: Meridional distributions of mixing fractions for (a) tropical tropospheric, (b) high-latitude stratospheric (through the shallow branch of the BDC), (c) high-latitude stratospheric (through the deep branch of the BDC), (d) mid-latitude LT, (e) high-latitude LT, and (f) the unclassified air masses estimated for January. Black contours indicate monthly averaged potential vorticity during the period from 2012 to 2016.

Atmos. Chem. Phys. Discuss., https://doi.org/10.5194/acp-2018-1030
Manuscript under review for journal Atmos. Chem. Phys.
Discussion started: 26 November 2018

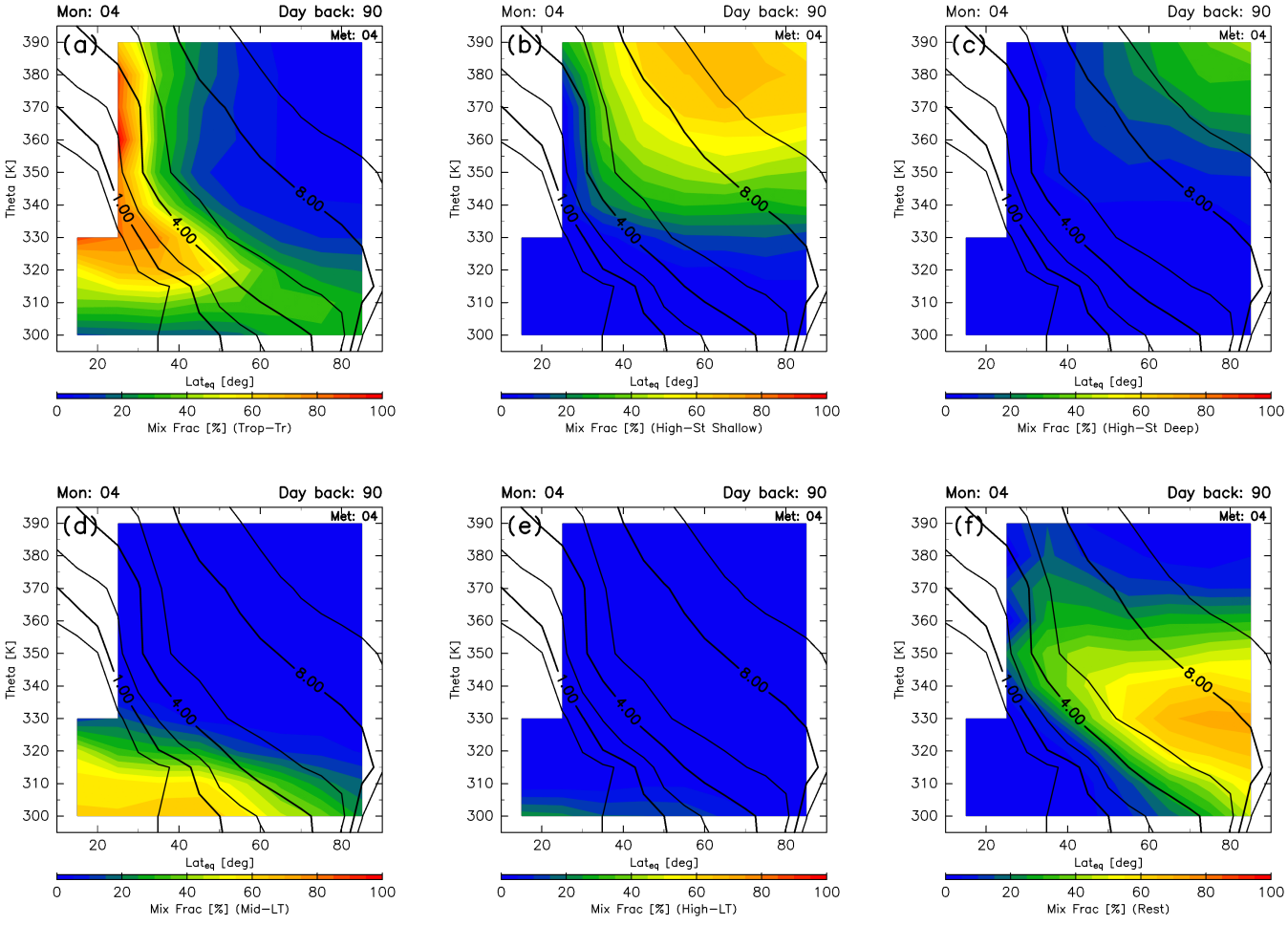

Figure 4: Same as Fig. 3, but for April.

Atmos. Chem. Phys. Discuss., https://doi.org/10.5194/acp-2018-1030
Manuscript under review for journal Atmos. Chem. Phys.
Discussion started: 26 November 2018

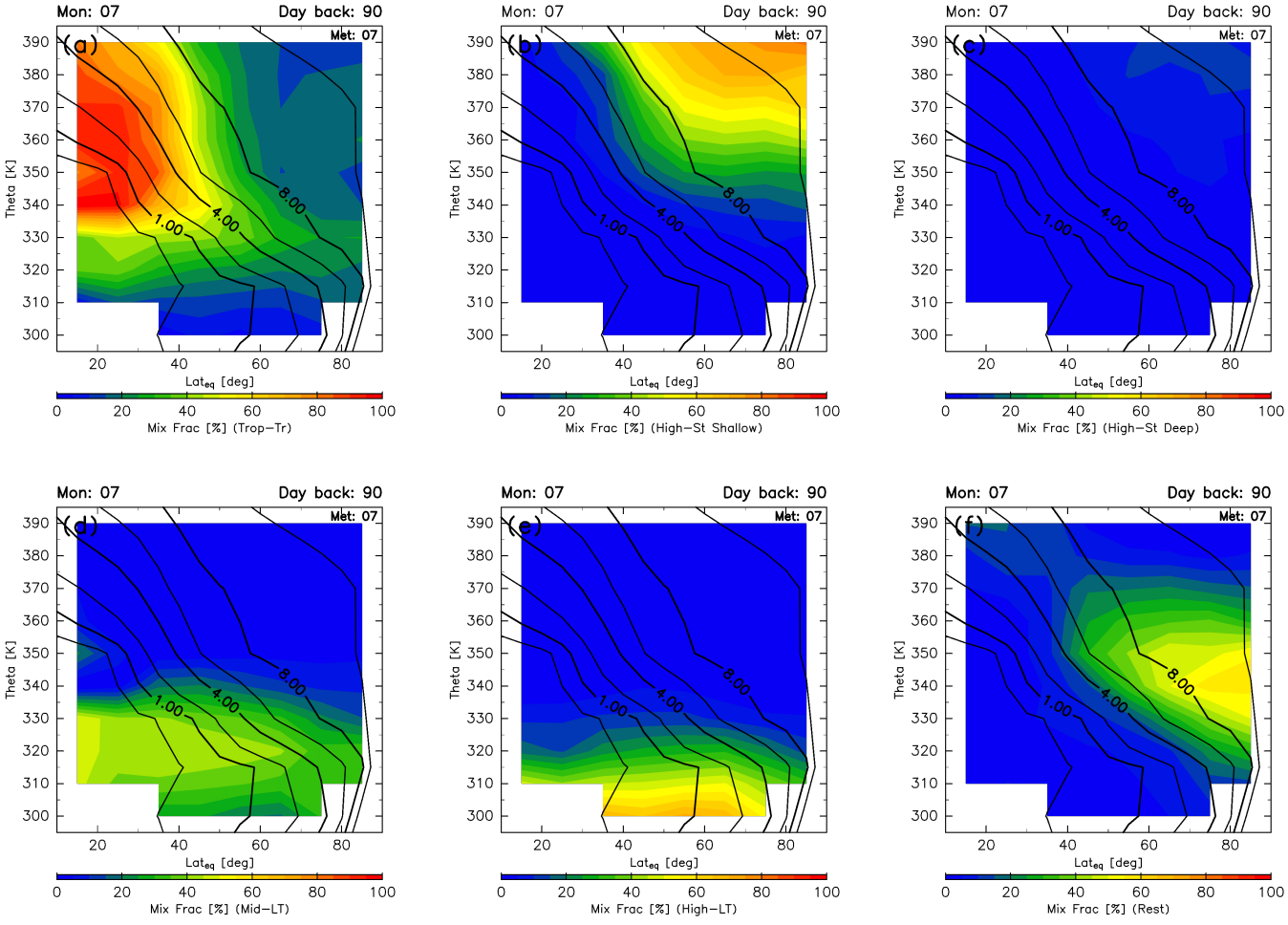

Figure 5: Same as Fig. 3, but for July.

Atmos. Chem. Phys. Discuss., https://doi.org/10.5194/acp-2018-1030
Manuscript under review for journal Atmos. Chem. Phys.
Discussion started: 26 November 2018

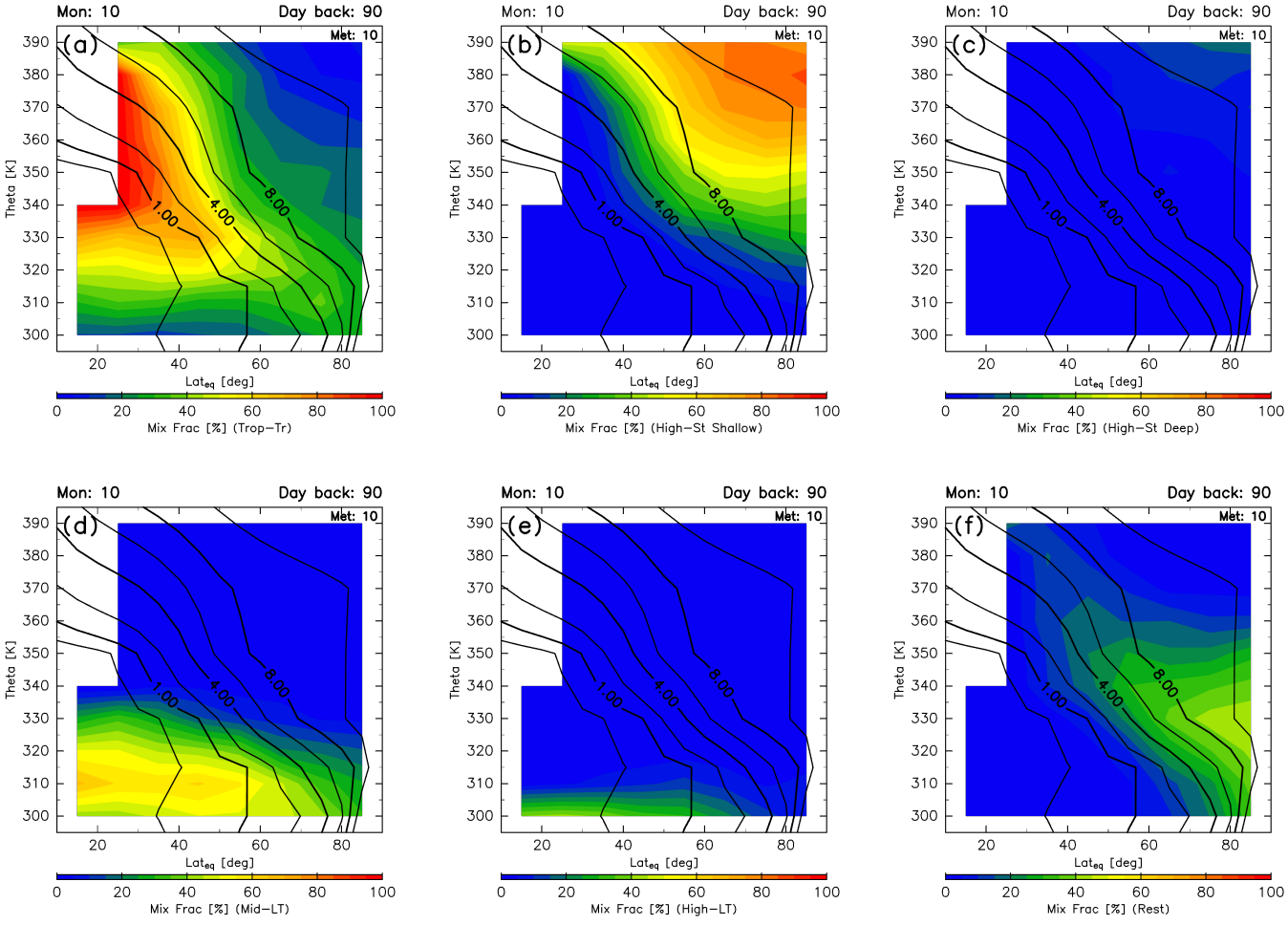

Figure 6: Same as Fig. 3, but for October.

Atmos. Chem. Phys. Discuss., https://doi.org/10.5194/acp-2018-1030
Manuscript under review for journal Atmos. Chem. Phys.
Discussion started: 26 November 2018

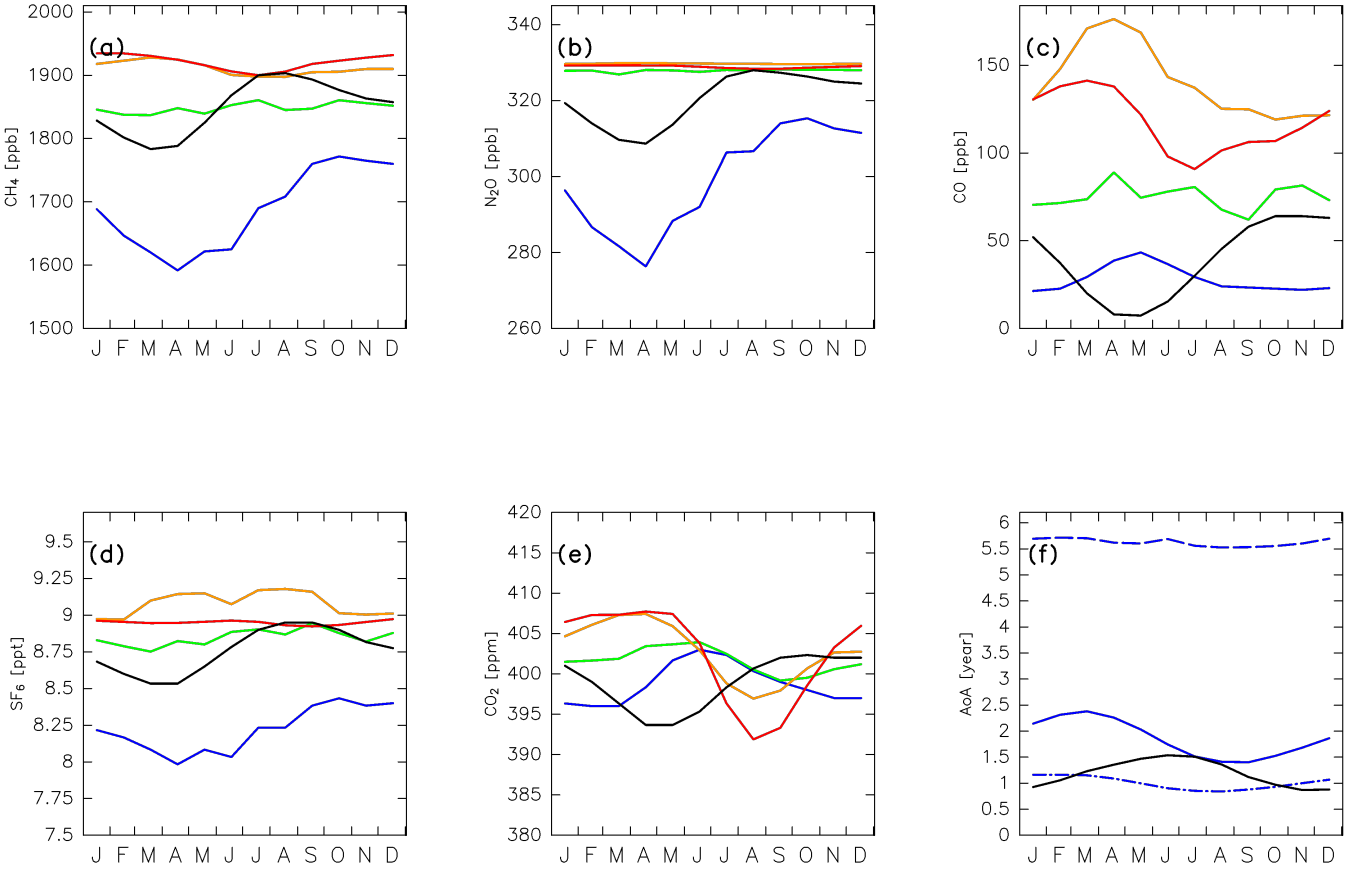

Figure 7: Seasonal variations in (a) CH_4, (b) N_2O, (c) CO, (d) SF_6, and (e) CO_2 mixing ratios estimated for (green) tropical tropospheric, (blue) high-latitude stratospheric, (orange) mid-latitude LT, (red) high-latitude LT, and (black) unclassified air masses. Seasonal variations in the age of air estimated for (blue solid) high-latitude stratospheric and (black) unclassified air masses are shown in (f). The dashed–dotted and dashed lines in (f) show the age of air separately estimated for high-latitude stratospheric air masses that travelled via the shallow and deep branches of the BDC, respectively.

Atmos. Chem. Phys. Discuss., https://doi.org/10.5194/acp-2018-1030
Manuscript under review for journal Atmos. Chem. Phys.
Discussion started: 26 November 2018

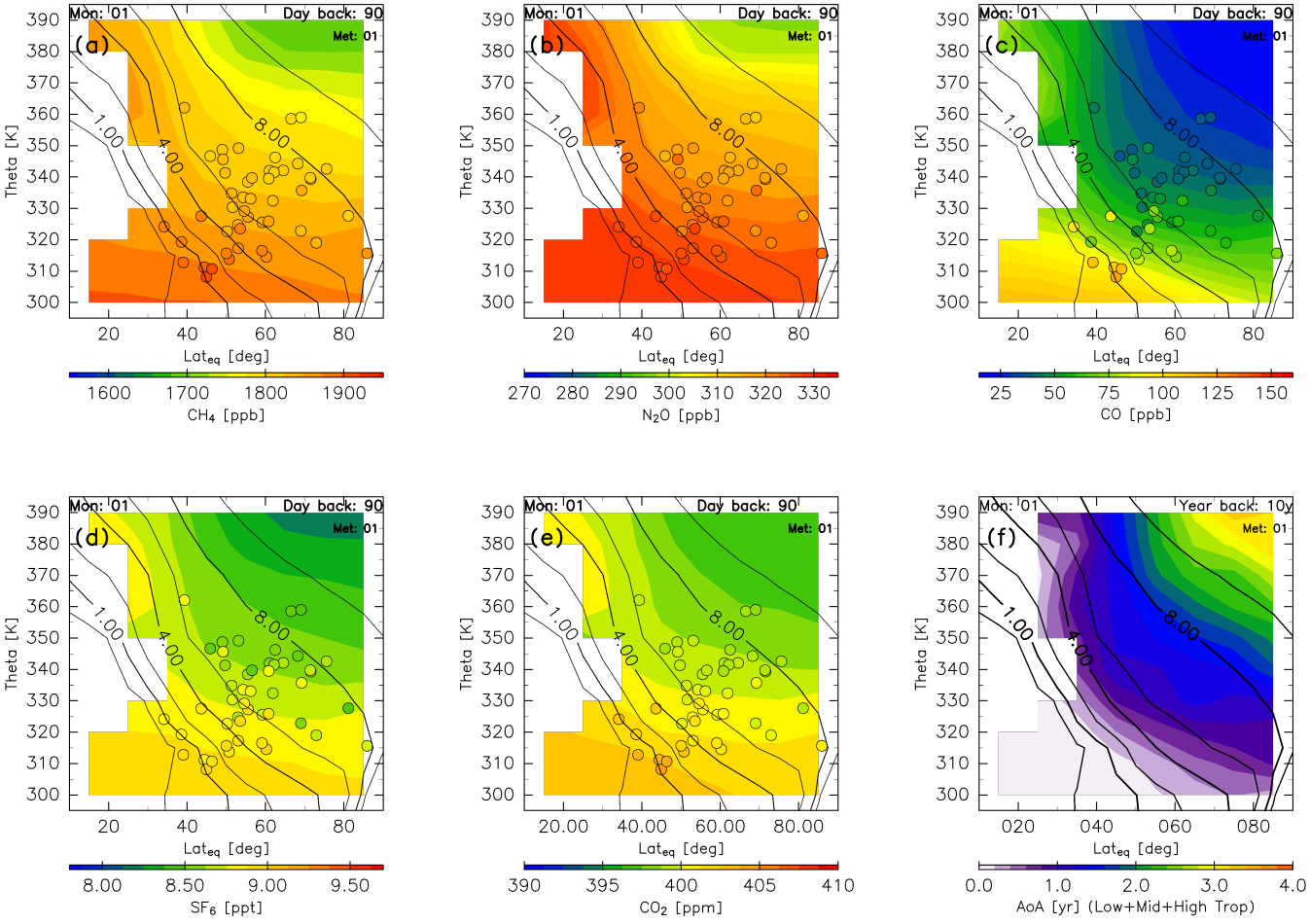

Figure 8: Meridional distributions of reconstructions for (a) CH_4, (b) N_2O, (c) CO, (d) SF_6, and (e) CO_2 for January. Detrended CONTRAIL measurements in April are plotted as circles using the same colour scale. The distribution of the age of air estimated for January is shown in (f). Black contours indicate monthly averaged potential vorticity during the period from 2012 to 2016.

5

Atmos. Chem. Phys. Discuss., https://doi.org/10.5194/acp-2018-1030
Manuscript under review for journal Atmos. Chem. Phys.
Discussion started: 26 November 2018

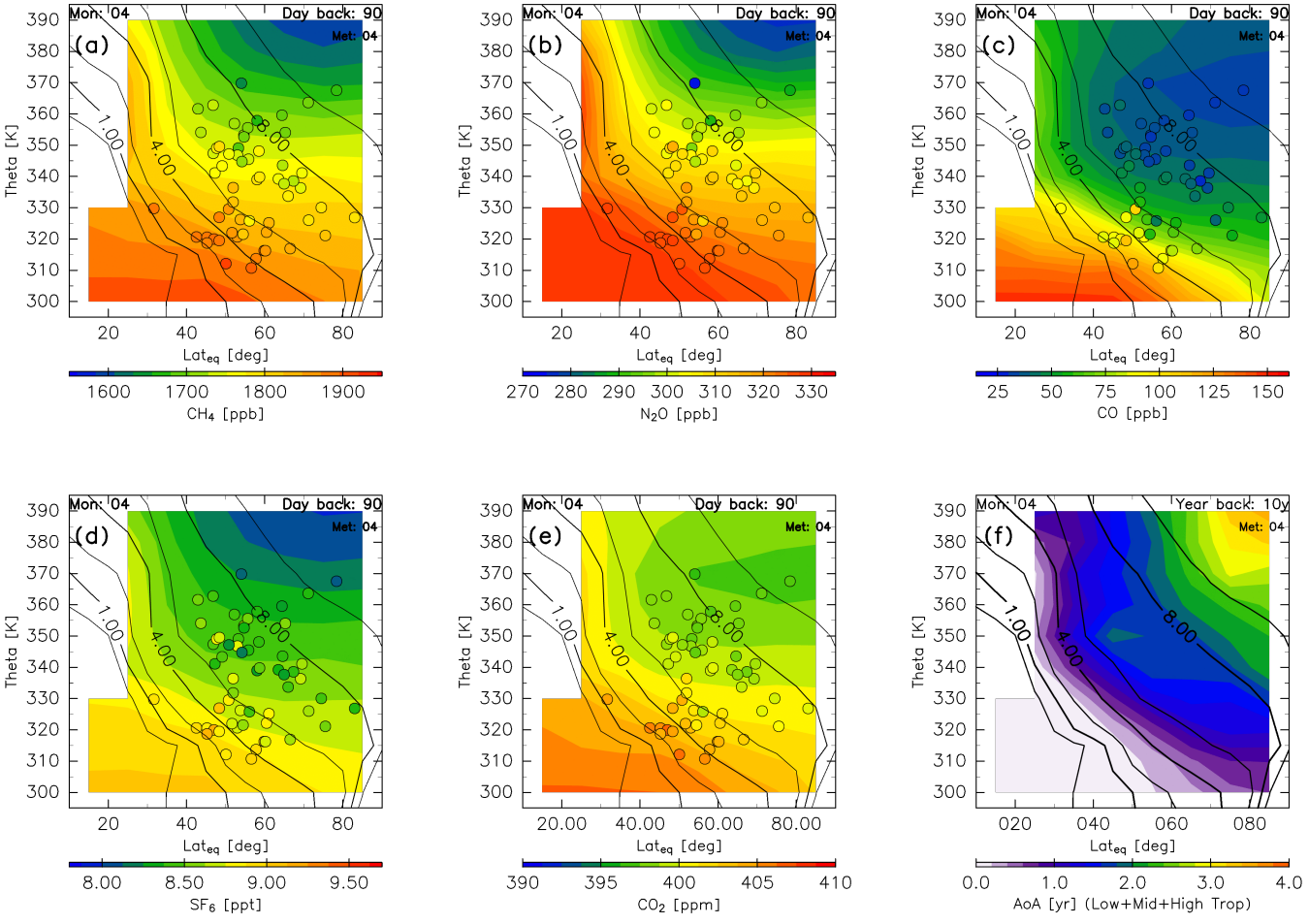

Figure 9: Same as Fig. 8, but for April.

Atmos. Chem. Phys. Discuss., https://doi.org/10.5194/acp-2018-1030
Manuscript under review for journal Atmos. Chem. Phys.
Discussion started: 26 November 2018

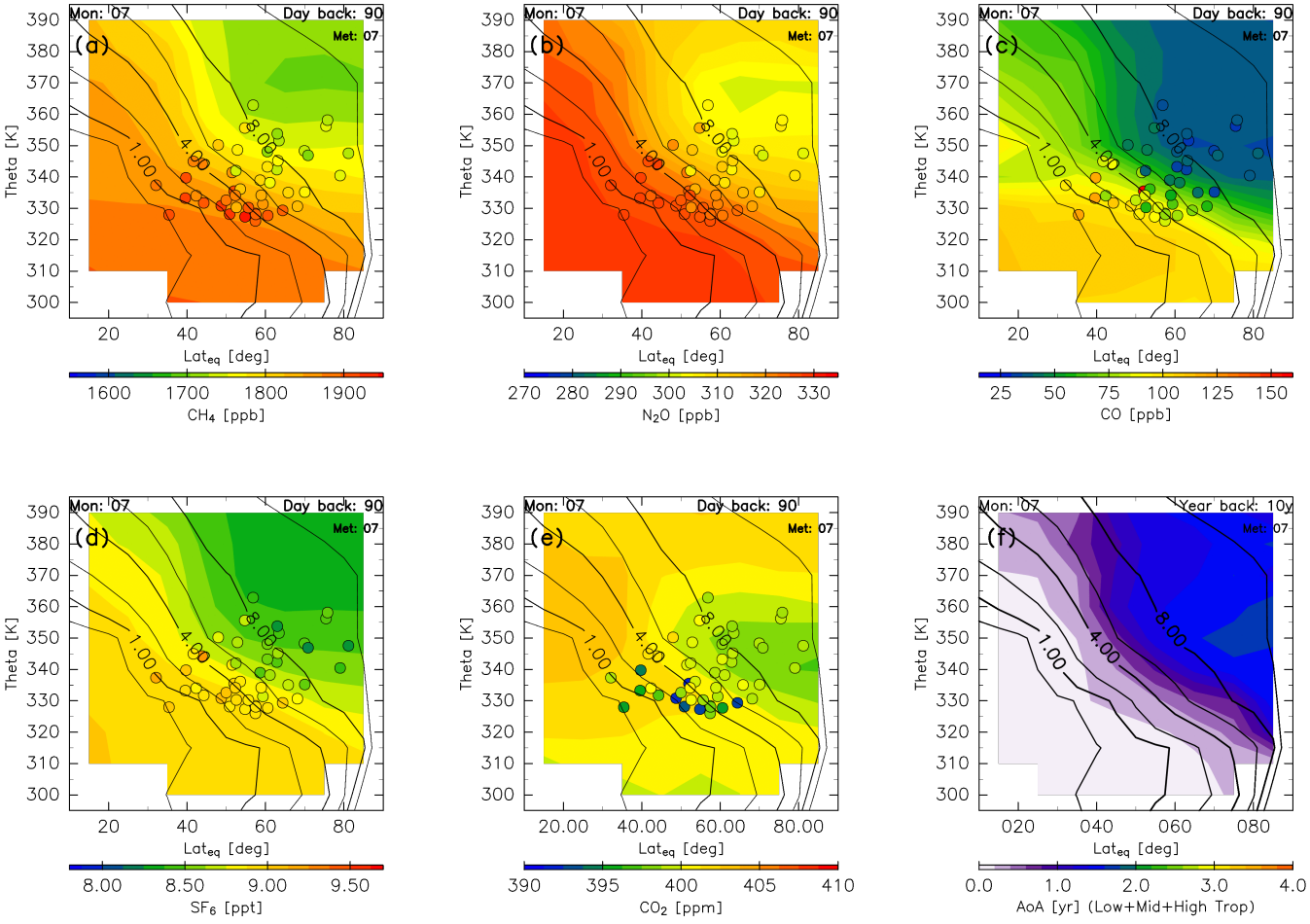

Figure 10: Same as Fig. 8, but for July.

Atmos. Chem. Phys. Discuss., https://doi.org/10.5194/acp-2018-1030
Manuscript under review for journal Atmos. Chem. Phys.
Discussion started: 26 November 2018

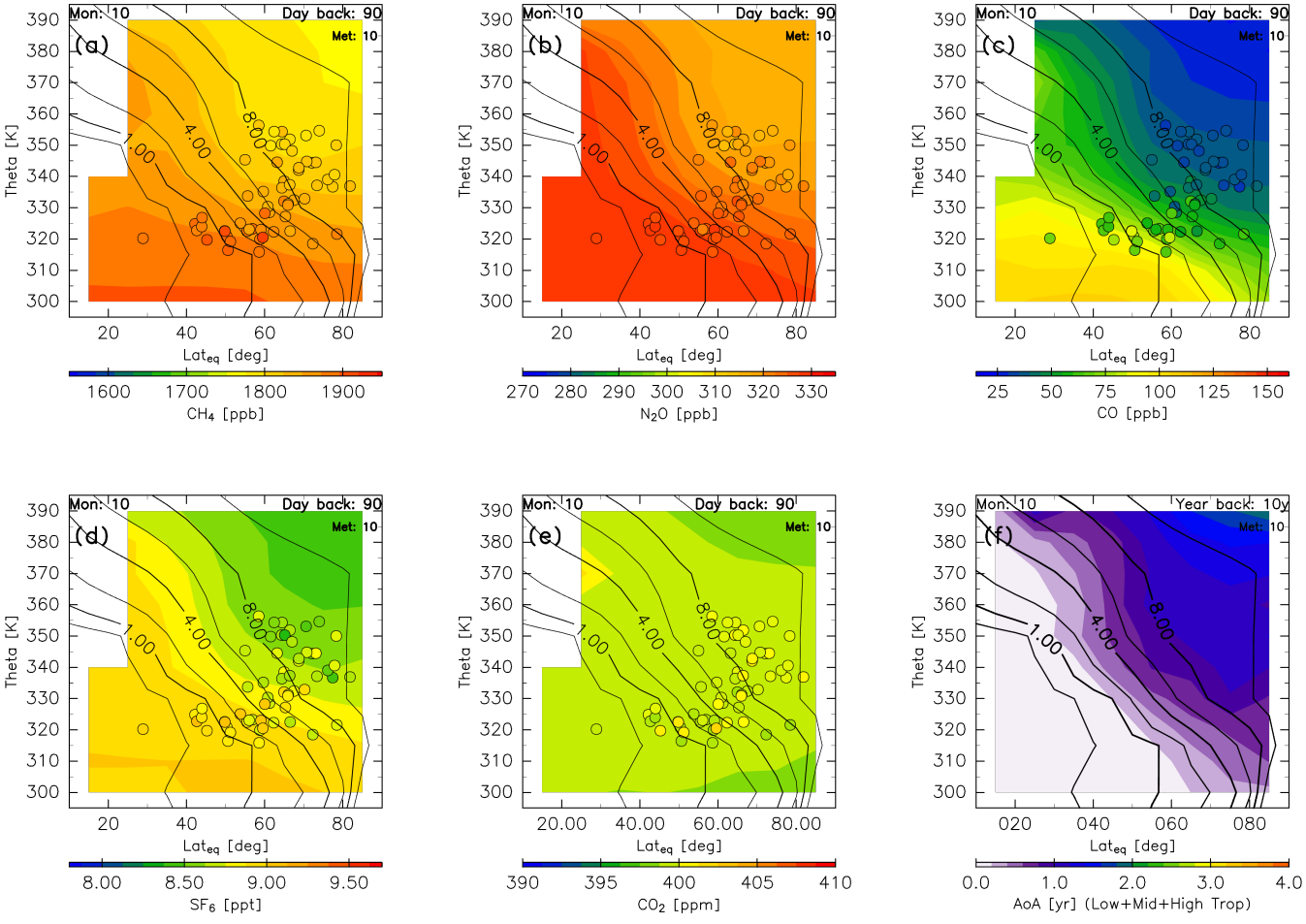

Figure 11: Same as Fig. 8, but for October.

Atmos. Chem. Phys. Discuss., https://doi.org/10.5194/acp-2018-1030
Manuscript under review for journal Atmos. Chem. Phys.
Discussion started: 26 November 2018

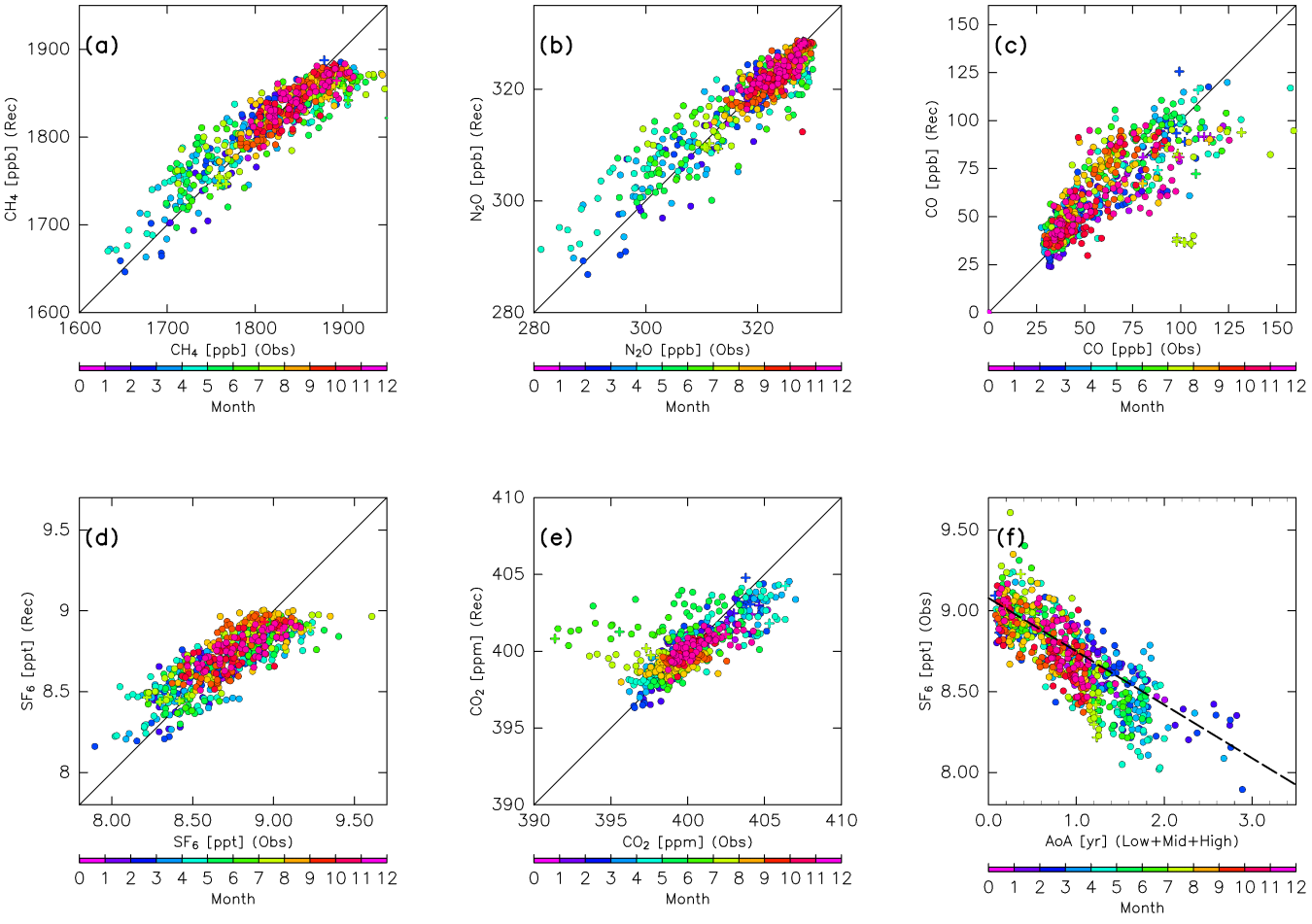

Figure 12: Scatter plots of CONTRAIL measurements versus reconstructions for (a) CH_4, (b) N_2O, (c) CO, (d) SF_6, and (e) CO_2, and (f) the age of air versus SF_6 measured by CONTRAIL. Colours indicate the month, and the dashed line in (f) shows the sign-reversed trend in tropospheric SF_6 (−0.33 ppt/year) with the intercept of the annual averaged mixing ratio at mid-latitudes for 2016 (9.08 ppt).

Atmos. Chem. Phys. Discuss., https://doi.org/10.5194/acp-2018-1030
Manuscript under review for journal Atmos. Chem. Phys.
Discussion started: 26 November 2018

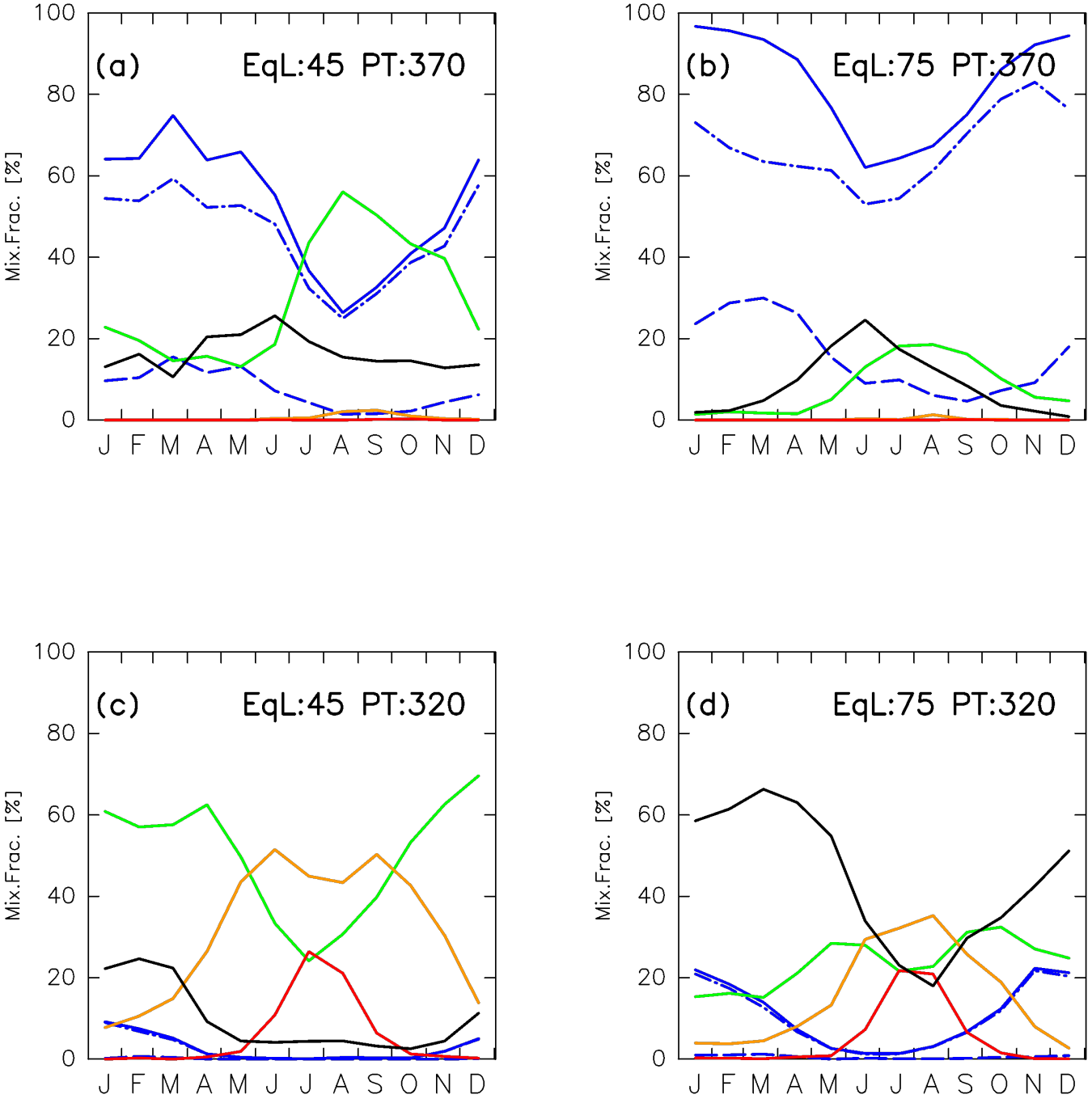

Figure 13: Seasonal variations in (green) tropical tropospheric, (blue) high-latitude stratospheric, (orange) mid-latitude LT, (red) high-latitude LT, and (black) unclassified mixing fractions estimated for the (a) mid-latitude upper ($\emptyset_{eq}$ = 45°N; θ = 370 K), (b) high-latitude upper ($\emptyset_{eq}$ = 75°N; θ = 370 K), (c) mid-latitude lower ($\emptyset_{eq}$ = 45°N; θ = 320 K), and (d) high-latitude lower ($\emptyset_{eq}$ = 75°N; θ = 320 K) ExUTLS. The blue dashed–dotted and dashed lines show the mixing fractions of high-latitude stratospheric air masses that travelled through the shallow and deep branches of the BDC, respectively.

Atmos. Chem. Phys. Discuss., https://doi.org/10.5194/acp-2018-1030
Manuscript under review for journal Atmos. Chem. Phys.
Discussion started: 26 November 2018

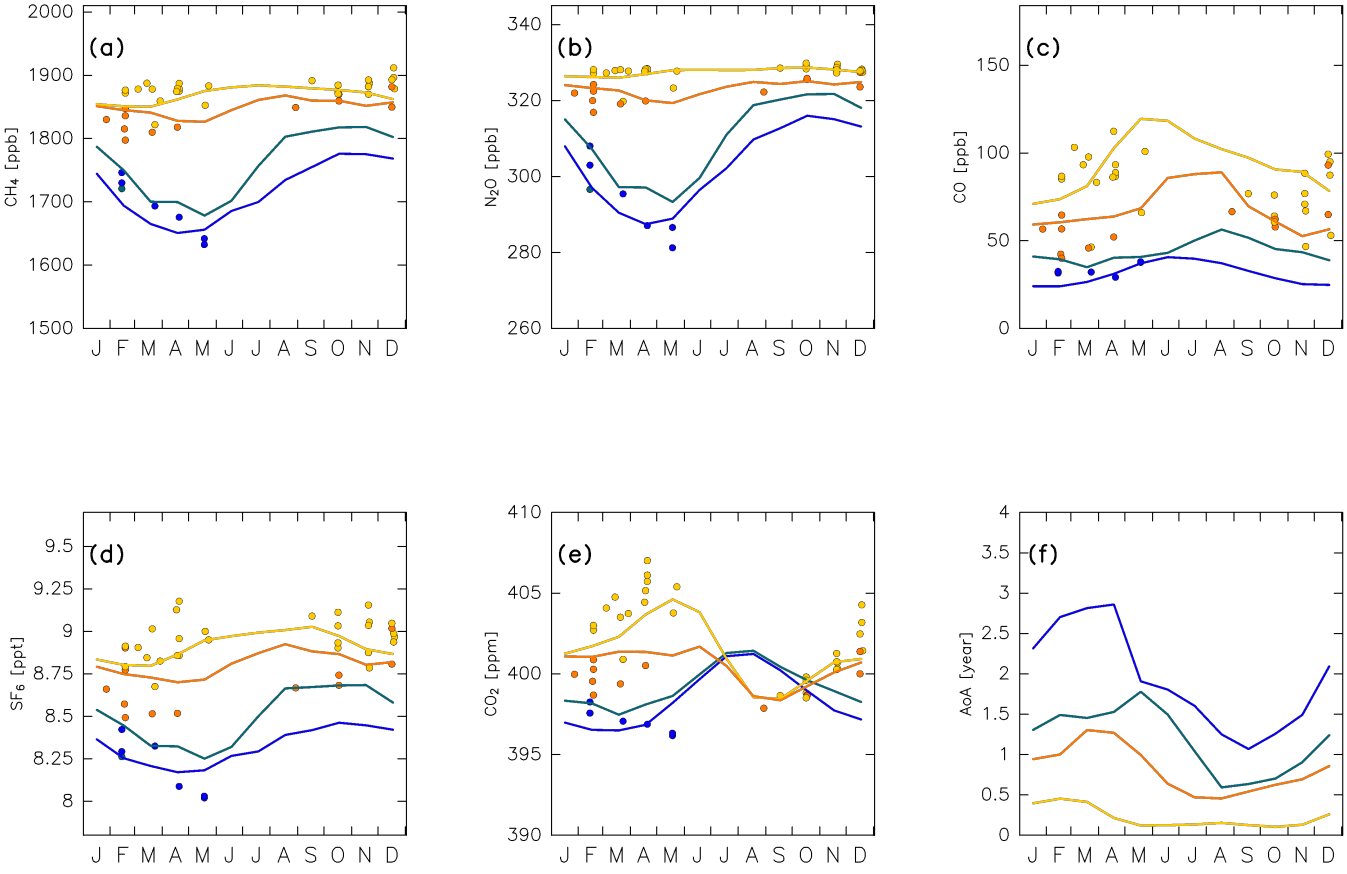

Figure 14: Seasonal variations in (a) CH_4, (b) N_2O, (c) CO, (d) SF_6, and (e) CO_2 mixing ratios estimated for the (green) mid-latitude upper ($\emptyset_{eq} = 45°N$; $\theta = 370$ K), (blue) high-latitude upper ($\emptyset_{eq} = 75°N$; $\theta = 370$ K), (yellow) mid-latitude lower ($\emptyset_{eq} = 45°N$; $\theta = 320$ K), and (orange) high-latitude lower ($\emptyset_{eq} = 75°N$; $\theta = 320$ K) ExUTLS superimposed on the detrended CONTRAIL measurements, which are color-coded according to measurements within ±5° in equivalent latitude and ±5 K in potential temperature of the reconstruction regions. Seasonal variations of the age of air estimated for the same locations are shown in (f).

Atmos. Chem. Phys. Discuss., https://doi.org/10.5194/acp-2018-1030
Manuscript under review for journal Atmos. Chem. Phys.
Discussion started: 26 November 2018

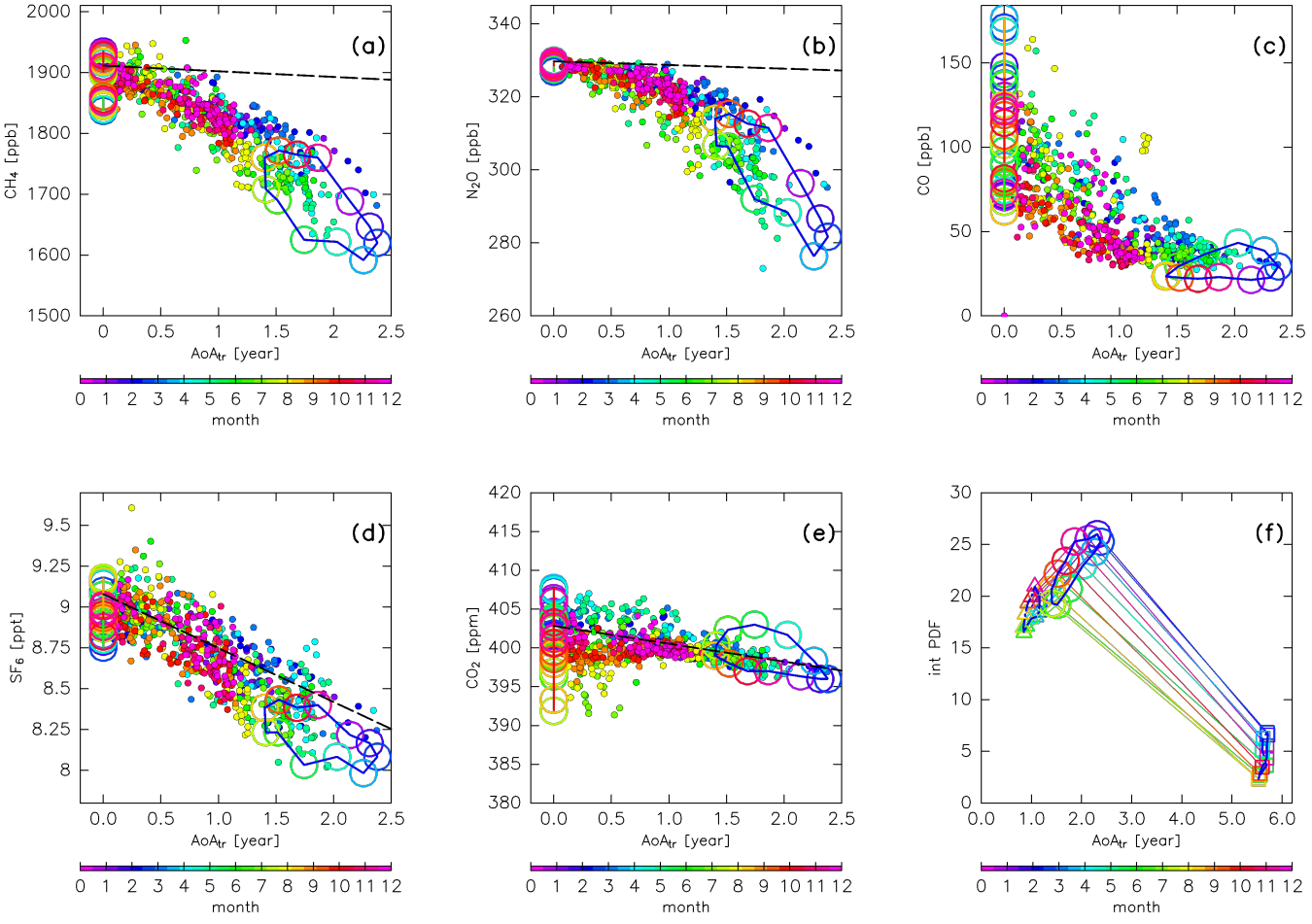

Figure 15: Scatter plots of the mean age of air versus (a) CH_4, (b) N_2O, (c) CO, (d) SF_6, and (e) CO_2 mixing ratios measured by CONTRAIL (filled circles; colours indicate the month). Lines with open circles, coloured according to month, show the original compositions for (green) tropical tropospheric, (blue) high-latitude stratospheric, (orange) mid-latitude LT, and (red) high-latitude LT air masses. Dashed lines in (a), (b), (d), and (e) show the sign-reversed trends of tropospheric CH_4 (−9.3 ppb/year), N_2O (−1.0 ppb/year), SF_6 (−0.33 ppt/year), and CO_2 (−2.3 ppm/year) with intercepts of the annual averaged mixing ratios at mid-latitudes for 2016 (1911 ppb, 330 ppb, 9.08 ppt, and 403 ppm), respectively. Panel (f) shows the mean age of air estimated for air masses originating in the high-latitude stratosphere (open circles), along with those estimated only for air masses passing through the deep (squares) and shallow branches (triangles) of the BDC. The ordinate is the integral of PDF for each subset.

Atmos. Chem. Phys. Discuss., https://doi.org/10.5194/acp-2018-1030
Manuscript under review for journal Atmos. Chem. Phys.
Discussion started: 26 November 2018

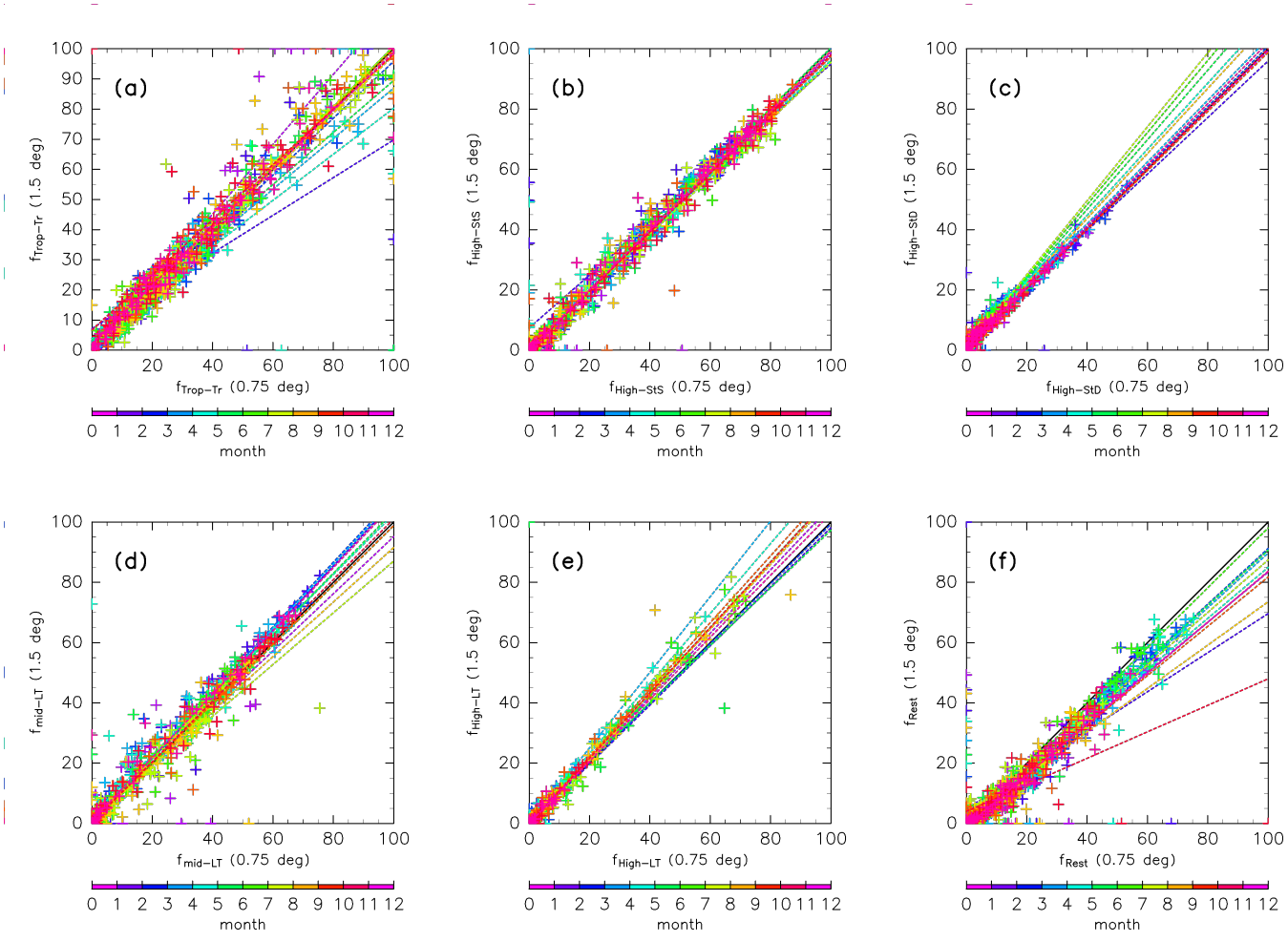

Figure A1: Scatter plots of mixing fractions calculated using ERA-Interim data with a horizontal resolution of 0.75° and 60 model levels versus those with 1.5° horizontal resolution and 37 pressure levels. Crosses indicate mixing fractions evaluated for all bins in the $\emptyset_{eq}$–θ cross-sections shown in Figs 3–6 for (a) tropical tropospheric, (b) high-latitude stratospheric (through the shallow branch of the BDC), (c) high-latitude stratospheric (through the deep branch of the BDC), (d) mid-latitude LT, (e) high-latitude LT, and (f) unclassified air masses. Colours indicate the month and dotted lines indicate the regression line for each month.

Atmos. Chem. Phys. Discuss., https://doi.org/10.5194/acp-2018-1030
Manuscript under review for journal Atmos. Chem. Phys.
Discussion started: 26 November 2018

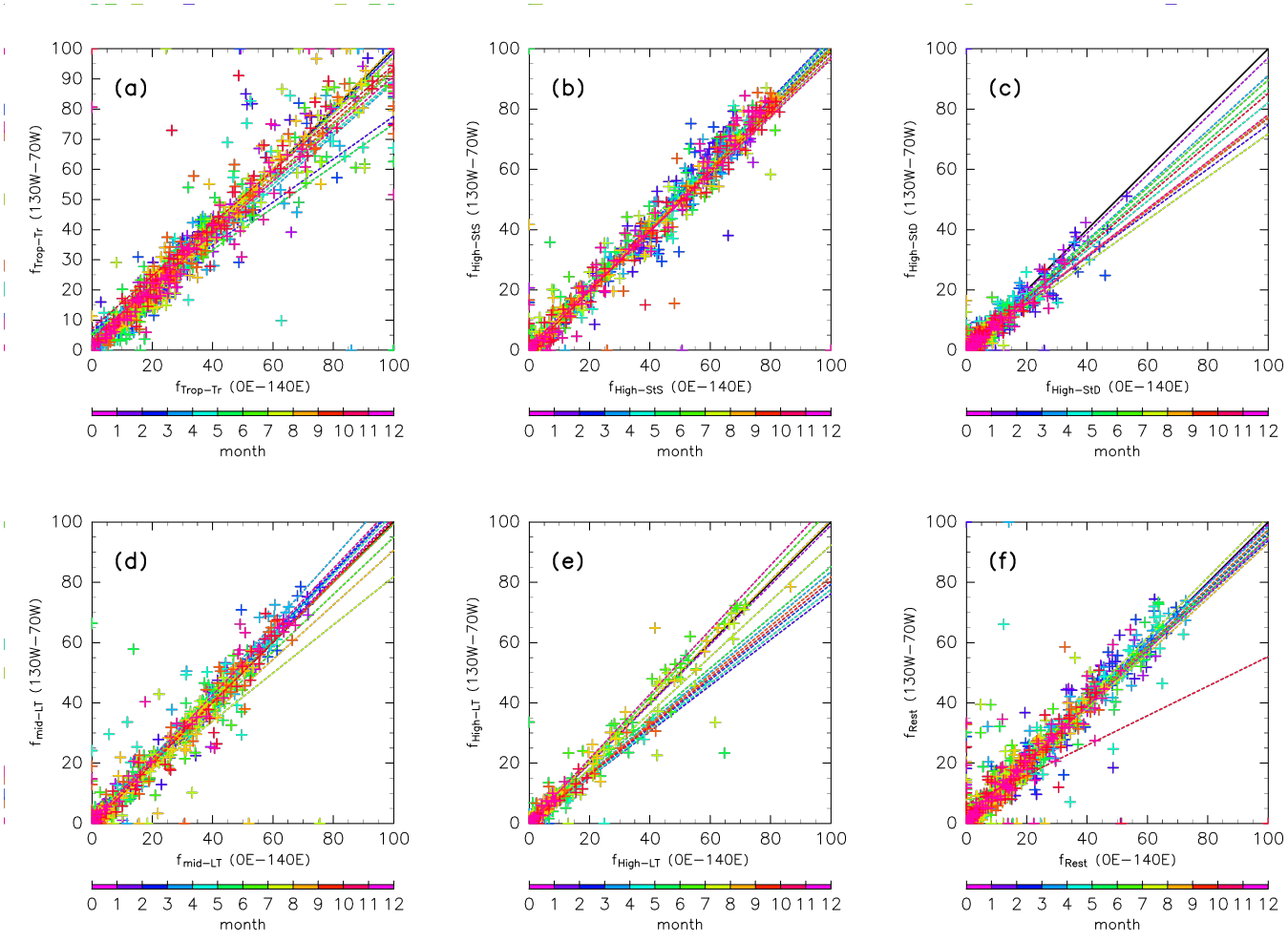

Figure A2: Same as Fig. A1, but for mixing fractions calculated for the longitudinal region within 0° E–140° E (default) versus those for the region within 130° W–70° W.